Supplemental material to this article can be found at:
http://jpet.aspetjournals.org/content/suppl/2019/04/15/jpet.119.256487.DC1

1521-0103/370/3/876–893$35.00
THE JOURNAL OF PHARMACOLOGY AND EXPERIMENTAL THERAPEUTICS
Copyright © 2019 by The American Society for Pharmacology and Experimental Therapeutics
https://doi.org/10.1124/jpet.119.256487
J Pharmacol Exp Ther 370:876–893, September 2019

The Journal of PHARMACOLOGY And Experimental Therapeutics

Special Section on Drug Delivery Technologies

Ultrasound-Triggered Spatiotemporal Delivery of Topotecan and Curcumin as Combination Therapy for Cancer[S]

Chandrashekhar Prasad and Rinti Banerjee

Department of Biosciences and Bioengineering, Indian Institute of Technology, Bombay, Mumbai, India

Received January 12, 2019; accepted April 8, 2019

ABSTRACT

Chemotherapy is limited by the low availability of drug at the tumor site and drug resistance by the tumor. In this report we describe a combination therapy for codelivery of two anticancer drugs with spatiotemporal control by ultrasound pulses. We developed curcumin and topotecan–coencapsulated nanoconjugates Cur_Tpt_NC.MB to have an ultrasound contrast property. MDA MB 231 and B16F10 cells were incubated with Cur_Tpt_NC.MB and exposed to ultrasound. Ultrasound exposure reduced the IC_{50} concentration of topotecan and curcumin significantly ($P < 0.05$) compared with free drug. Antitumor efficacy study of the Cur_Tpt_NC.MB in B16F10 melanoma tumor–bearing C57BL/6 mice showed that ultrasound exposure of right tumor reduced growth by 3.5 times compared with the unexposed left tumor of same mice and 14.8 times compared with a group treated with a physical mixture of drugs. These results suggest that the nanotherapeutic system we developed induces site-specific inhibition of tumor growth at a high rate and has the potential to be used as a therapeutic regimen for spatiotemporal delivery of dual drugs for treatment of cancer.

Introduction

Trigger-based modalities of drug delivery have a beneficial edge over conventional chemotherapy as on-demand release of drug from nanoparticles is catalyzed by either the microenvironment of the tumor (viz., pH, overexpressed enzymes, hyperthermia) or by site-specific exposure to external agents (viz., ultrasound, magnetic field, photon) that enhance the payload drug at the tumor site and minimize systemic toxicity (Mura et al., 2013; Ordeig et al., 2016; Zhu et al., 2016). Ultrasound is a minimally invasive well established diagnostic agent and is being evaluated for its therapeutic efficacy all across the world. In ultrasound-mediated delivery of cargo, the ultrasound contrast agent (UCA) plays a very crucial role; the sulfur hexafluoride gas (SF_6)–containing lipid-shelled microbubble (MB) is the most widely studied UCA (Cosgrove, 2006; Lv et al., 2016). Ultrasound-induced stable and inertial cavitation of MB leads to jet propulsion of the surrounding fluid, which in turn exerts shear stress on the membranes of cells situated nearby and facilitates intracellular delivery through creation of transient pores (Ferrara, 2008; Zhou et al., 2012; Liu et al., 2014). Furthermore, lipid-shelled MB and doxorubicin (DOX)-encapsulated liposome conjugates have been shown to increase the cytotoxicity of DOX in BLM melanoma cells following exposure to ultrasound (Lentacker et al., 2010; Geers et al., 2011).

Topotecan (Tpt) is a water-soluble analog of camptothecin, an anticancer drug that blocks replication of DNA by inhibiting topoisomerase I activity. At neutral pH, Tpt is sparingly soluble in aqueous medium and, moreover, it ionizes from lactone to carboxylate form (Fassberg and Stella, 1992;

The project was funded by Samsung Global Research Outreach (GRO) program.
https://doi.org/10.1124/jpet.119.256487.
[S] This article has supplemental material available at jpet.aspetjournals.org.

ABBREVIATIONS: B16F10, B16 melanoma F10 cells; CLSM, Confocal laser scanning microscope; Cur, curcumin; Cur_NC, Cur-encapsulating nanocapsule; Cur_NC.MB, nanoconjugates of Cur_NC and microbubbles; Cur_NE, Cur nanoemulsions; Cur_Tpt_NC, Cur and Tpt–coencapsulating nanocapsules; Cur_Tpt_NC.MB, Cur and Tpt coencapsulating nanocapsule and microbubble nanoconjugates; DMEM, Dulbecco's modified Eagle's medium; DOPS-Na, 1, 2-dioleoyl-*sn*-glycero-3-phosphoserine; DSPC, 1, 2-distearoyl-*sn*-glycero-3-phosphocholine; EDC, ethyl (dimethylaminopropyl) carbodiimide hydrochloride; EE, encapsulation efficiency; FBS, fetal bovine serum; FITC, fluorescein isothiocyanate; FTIR, Fourier-transform infrared spectroscopy; HPLC, high-performance liquid chromatography; MB, microbubble; MB-ND, Nile red-loaded MB; MDA MB 231, M. D. Anderson metastatic breast cancer cell; MTD, maximum tolerated dose; MTT, 3-(4, 5-dimethylthiazol-2-yl)-2, 5-diphenyltetrazolium bromide; MQ, Milli-Q water; NC, nanocapsules; NC_B, blank nanocapsules; NC_B.MB, blank nanocapsules and MB nanoconjugates; NC-FITC, FITC-stained nanocapsules; NC-FITC.MB-ND, covalent nanoconjugates of NC-FITC and MB-ND; NC-Rh6g, rhodamine 6g-encapsulating nanocapsules; NHS, *N*-hydroxysuccinimide; PBS, Dulbecco's phosphate-buffered saline 1×; PI, propidium iodide; Rh6g, rhodamine 6g; SF_6, sulfur hexafluoride gas; TPGS, D-α-tocopheryl polyethylene glycol 1000 succinate; Tpt, topotecan; Tpt_NC, Tpt-encapsulating nanocapsules; Tpt_NC.MB, nanoconjugates of Tpt_NC and microbubbles.

Downloaded from jpet.aspetjournals.org at ASPET Journals on April 10, 2024

Drummond et al., 2010). This ionic transformation diminishes the anticancer activity of Tpt and its solubility at physiological pH in aqueous medium (Fassberg and Stella, 1992; Drummond et al., 2010). Encapsulation of Tpt inside liposome stabilized the drug and maintained its activity (Drummond et al., 2010). As far as the therapeutic efficacy of curcumin is concerned, poor aqueous solubility compromises its anticancer activity owing to inadequate cellular internalization. Encapsulation of Cur inside lipid or polymer-based nanoparticles has been found to enhance the cellular internalization and cytotoxicity of Cur (Rao et al., 2014).

Codelivery of hydrophobic and hydrophilic drugs in the same carrier with high entrapment has been a challenge. There have been no attempts to deliver multiple drugs via an ultrasound-responsive system for anticancer therapy. We describe here Tpt and Cur–coencapsulating nanocapsule (Cur_Tpt_NC) and MB nanoconjugate Cur_Tpt_NC.MB for ultrasound-triggered drug delivery in cancer. Having a hydrophobic core and hydrophilic polymeric shell, nanocapsules are more stable than liposomes, and hence nanoconjugates have the advantage of higher stability than microbubble-liposome complexes and are suitable for encapsulation of both hydrophobic and hydrophilic drugs. To the best of our knowledge, MB-nanocapsule nanoconjugates and ultrasound-mediated codelivery of hydrophobic and hydrophilic drugs have not been explored previously.

Materials and Methods

Materials

1-Ethyl-3-(3-dimethylaminopropyl) carbodiimide hydrochloride (EDC) (99%), *N*-hydroxysuccinimide (NHS) (>97%), 3-(4, 5-dimethylthiazol-2-yl)-2, 5-diphenyltetrazolium bromide (MTT) (assay 98%–102%), 2-(*N*-morpholino) ethanesulfonic acid anhydrous (MES) (assay 99%–102%), Dulbecco's modified Eagle's medium (DMEM), trypsin-EDTA 1×, Dulbecco's phosphate-buffered saline 1× (PBS), lecithin (Soya) (30%), dialysis membrane-50, fetal bovine serum (FBS), antibiotic-antimycotic solution 100×, curcumin (97%) were purchased from Himedia Laboratories Pvt. Ltd, India. 1, 2-Distearoyl-sn-glycero-3-phosphocholine (DSPC) (99%) and 1,2 -dioleoyl-sn-glycero-3-phosphoserine (sodium slat) (DOPS-Na) (99%) were purchased from Lipoid GmbH, Germany. Rhodamine 6G (Rh6g) (99%), propidium iodide (PI) (≥94%), D-α-tocopheryl polyethylene glycol 1000 succinate (TPGS) (96%), Nile red (≥98%), and fluorescein isothiocyanate (FITC) (≥90%), were purchased from Sigma-Aldrich. Topotecan (99%) was purchased from Fresenius Kabi India Pvt. Ltd. AnnexinV-FITC was purchased from Invitrogen, ThermoFisher Scientific Inc. Chitosan (85% deacetylation, M_w approx. 7000 kDa) was procured from Marine chemicals, India. All solvents were of high-performance liquid chromatography (HPLC) grade and procured from Merck Life Science Pvt. Ltd., India. Sulfur hexafluoride was obtained from Med Gas N equipment, India. β-Glucuronidase (125 KU) was procured from Sigma-Aldrich.

Methods

Preparation of Nanocapsules and Microbubbles. Tpt and Cur–coencapsulated nanocapsules were prepared in two steps. In the first step, Cur nanoemulsions (Cur_NE) were prepared by the oil-in-water emulsion method followed by evaporation of solvent. In brief, 80 mg of lecithin and 10 mg of Cur were dissolved in 5 ml of chloroform and then 5 ml of acetone was added. This organic phase was poured into a 20-ml aqueous phase under stirring at 600 rpm. Then the emulsion was passed through a homogenizer (Avestin Emulsiflex C3 homogenizer) at 10,000–15,000 psi for three cycles, and thereafter solvent was evaporated to obtain the Cur_NE solution (Fig. 1A). In the second step, these Cur_NE were further coated with chitosan and Tpt to synthesize Cur_Tpt_NC. To coat the Cur_NE with chitosan and Tpt, 10 mg of Tpt was dissolved in the Cur_NE's solution, then 10 mg of chitosan, dissolved in 0.5% acetic acid solution, was added under continuous stirring (Fig. 1A). Solution was stirred for 1 hour and then centrifuged (SIGMA 3K-30 laboratory centrifuge) at 20,000*g* for 20 minutes. The pellet thus obtained contained Cur_Tpt_NC (Fig. 1A.a)

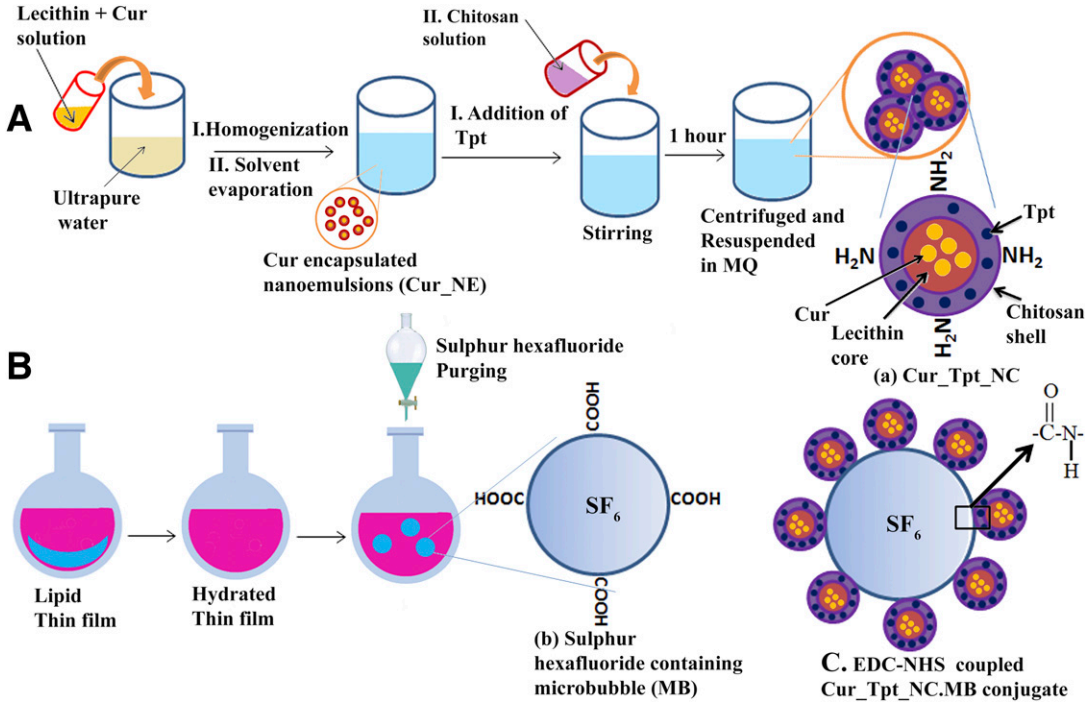

Fig. 1. Preparation of (A) nanocapsules (Cur_Tpt_NC) and (B) SF_6-encapsulated microbubbles (MB). (C) Schematic of Tpt and Cur-coencapsulated nanocapsule-microbubble nanoconjugates Cur_Tpt_NC.MB.

Downloaded from jpet.aspetjournals.org at ASPET Journals on April 10, 2024

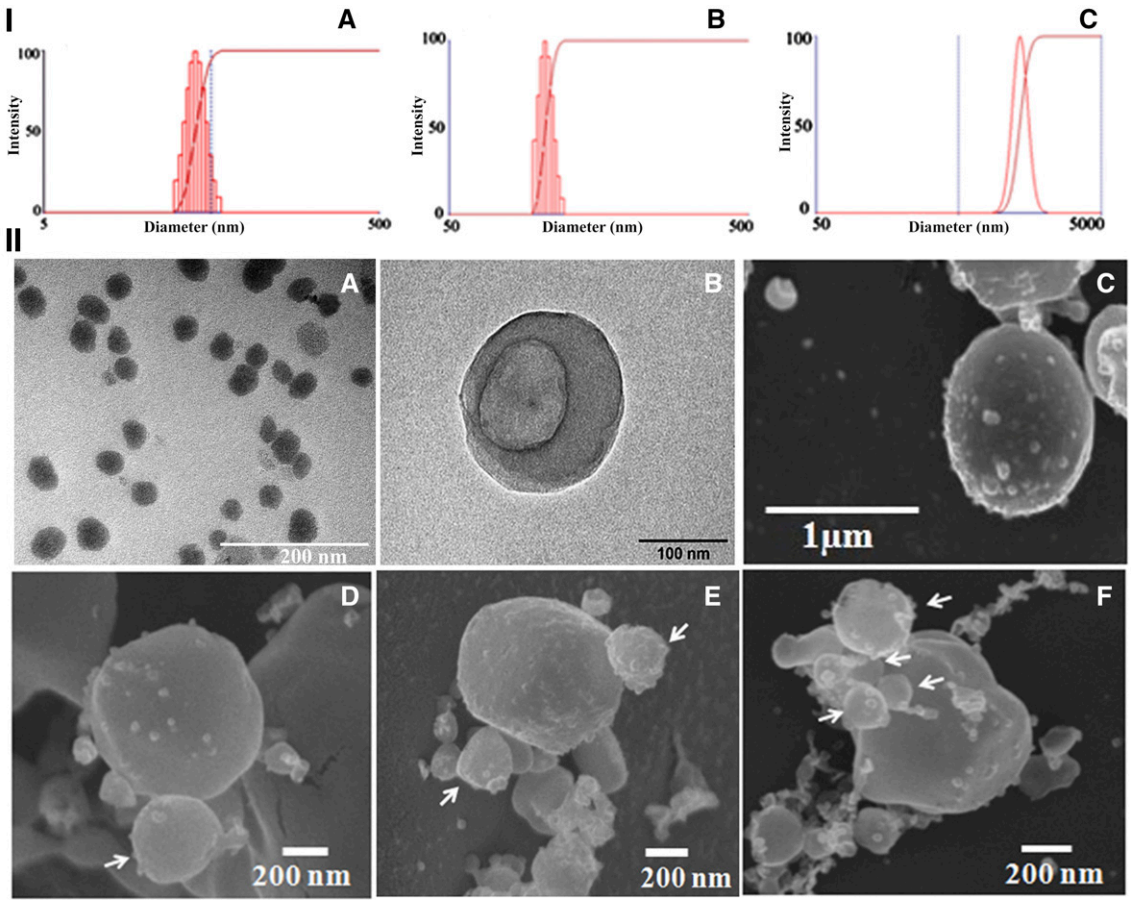

Fig. 2. I. Hydrodynamic size distribution of (A) Cur_NE, (B) Cur_Tpt_NC, and (C) MB. II. Electron microscope image of nanoparticles: transmission electron microscope images of (A) Cur_NE and (B) Cur_Tpt_NC. (C) SEM image of MB. (D–F) Field-emission-gun–scanning electron microscopy image of nanoconjugates Cur_Tpt_NC.MB. Central micrometer size particle represents MB and nanoscale particle adsorbed over its surface represents Cur_Tpt_NC (arrow).

and was resuspended in 2 ml of Milli-Q water (MQ). The supernatant was kept separately to estimate the amount of nonencapsulated Tpt and Cur. Supernatant was also used to estimate the amount of chitosan coated over the NE (Muzzarelli, 1998). The amount of encapsulated Tpt and Cur was measured by determining encapsulation efficiency (EE) using HPLC (JASCO International) through the indirect method, using the formula:

$$EE(\%) = \frac{Amount\ of\ drug\ taken(mg) - Amount\ of\ drug\ insupernatant(mg)}{Amount\ of\ drug\ taken(mg)} \times 100 \quad (1)$$

Blank nanocapsules (NC_B) were prepared in a similar way without addition of Cur and Tpt. For flow cytometry analysis, FITC-stained nanocapsules (NC-FITC) were prepared by dissolving 2 mg of FITC in the blank NE's solution and then chitosan was added. The rest of the process was similar to the preparation of NC_B. To synthesize rhodamine 6g-encapsulated nanocapsules (NC-Rh6g), 1 mg of Rh6g dye was dissolved in 5 ml of chloroform along with lecithin and then 5 ml of acetone was added. The rest of the process was similar to the preparation of NC_B.

SF_6 gas-containing MBs were prepared by thin film hydration method followed by purging of SF_6 with simultaneous agitation as shown in Fig. 1B. DSPC, DOPS-Na, and TPGS were dissolved in 5 ml of chloroform in a 20:1:1.5 molar ratio, and final concentration of lipid was maintained at 2 mg/ml. A thin film of lipid was developed in a round-bottomed flask using a rotatory evaporator at 50°C and then hydrated in 10 ml of PBS, pH 7.4, at 60°C for 1 hour. Two milliliters of hydrated lipid suspension was transferred to an Eppendorf tube and purged with SF_6 at a flow pressure of 0.5 kg/cm^2 for 30 seconds in sealed condition. The solution was further agitated for another 2 minutes using a vortex and kept undisturbed for 10–15 minutes, which led to its separation into three distinct layers (Supplemental Fig. S1). MBs contained the middle layer were isolated and analyzed for size and zeta potential. To estimate the amount of lipid from which MB was actually synthesized, the total amount of lipids present in this middle layer was estimated by ammonium ferrothiocyanate reagent (Stewart, 1980). It is documented that the bubbles residing in the uppermost layer are of larger size, and that is why they were not considered for further study (Xing et al., 2010). Likewise, the lowermost layer was also not selected for the study as it comprised the free lipid molecules that could not synthesize MB (Xing et al., 2010). Nile red-stained MBs (MB-ND) were prepared for flow cytometry analysis by dissolving 1 mg of Nile red in 5 ml of chloroform along with DSPC, TPGS, and DOPS-Na. The remainder of the process was similar to the preparation of blank MB.

Physiochemical Characterization. Both Cur_Tpt_NC and MB were diluted appropriately and characterized for their hydrodynamic diameter and zeta potential by DLS (Brookhaven DLS) and Zeta Potentiometer (Brookhaven), respectively. Intensity correlation functions were measured at a 90-degree angle, 25°C temperature, and 632-nm wavelength. Electron microscopic analysis was done to study the topography and diameter of the Cur_NE, Cur_Tpt_NC and MB. Both Cur_NE and Cur_Tpt_NC were negatively stained with 1% phosphotungstic acid (PTA) for transmission electron microscope (TEM) imaging. In TEM imaging Cur_NE and Cur_Tpt_NC were

Downloaded from jpet.aspetjournals.org at ASPET Journals on April 10, 2024

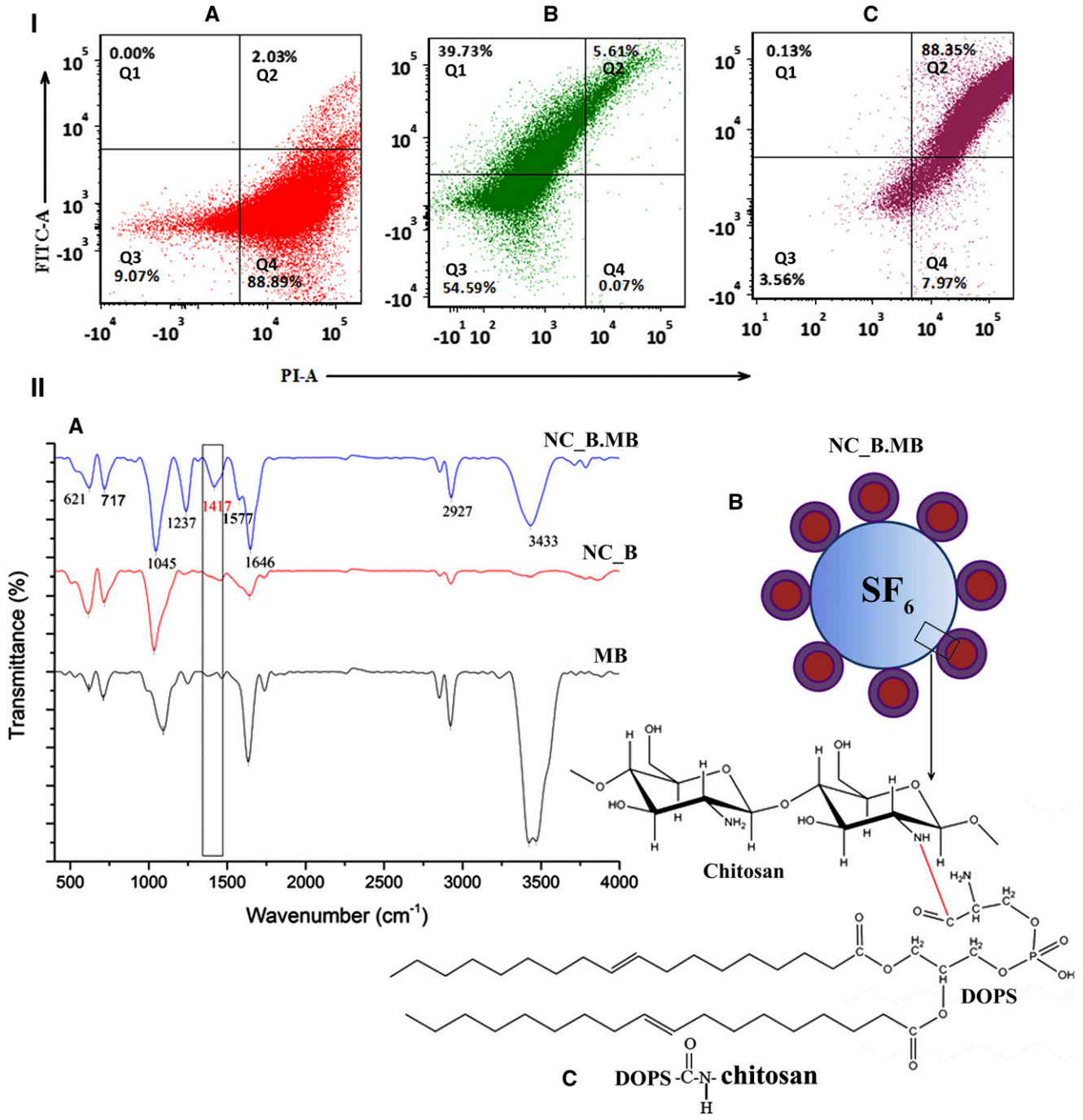

Fig. 3. I. Flow cytometry assay for determination of conjugation efficiency: (A) quadrant Q4 composed of Nile red-stained microbubbles (MB-ND); (B) FITC-stained nanocapsules (NC-FITC) occupied quadrant Q1 and Q3; (C) the nanoconjugates (NC-FITC.MB-ND) of MB-ND and NC-FITC occupied quadrant Q2. II. (A) FTIR spectrum of NC_B, MB, and NC_B.MB. New peak obtained at 1417 cm^{-1} in NC_B.MB corresponds to stretching vibration of newly synthesized C–N bond. (B) Schematic representation of NC_B.MB. (C) Chemical structure of conjugated chitosan and DOPS. The red line indicates newly synthesized amide bond between MB and NC_B. DOPS and chitosan are the constituents of MB and NC_B, respectively.

diluted appropriately and then 20 μl of sample was mixed with 20 μl of 1% PTA filtered solution. Thereafter 20 μl of PTA-stained samples were mounted carefully on copper TEM specimen-support grids. Grids were kept in desiccators for 12–14 hours and then analyzed. In scanning electron microscopic (SEM) analysis, the MB's concentration was diluted appropriately and frozen in liquid nitrogen. Frozen samples were sublimed at −90°C for 10 minutes and coated with platinum at a 10-mA current for 45 seconds before analysis.

Preparation of Nanoconjugates Cur_Tpt_NC.MB/NC_B.MB/NC-FITC.MB-ND/NC-Rh6g.MB. DOPS-Na present in MB provides a carboxylic group (Fig. 1B.b) and chitosan present in the Cur_Tpt_NC provides an amine group (Fig. 1A.a) for the amide bond synthesis via EDC-NHS coupling reaction (Bartczak and Kanaras, 2011). Briefly, stock solution of EDC (concentration: 4 mg/ml) and NHS (concentration: 11 mg/ml) was prepared in 0.1 M MES buffer (pH 6.0) supplemented with 0.5 M NaCl. Two hundred microliters of EDC solution was added first to 50 μl of MB solution (stock concentration: 3 mg/ml, with respect to lipid) and then 200 μl of NHS was added after 5 minutes. Thereafter, the reaction mixture was kept for 20 minutes on a rocker for end-to-end mixing. After 20 minutes

Downloaded from jpet.aspetjournals.org at ASPET Journals on April 10, 2024

100 μl of Cur_Tpt_NC (stock concentration: 1.25 mg/ml, with respect to chitosan) solution was added and then volume was adjusted to 1.0 ml using PBS. Reaction mixture was kept for 2 hours on the rocker for end-to-end mixing at room temperature. Remnants of activated EDC and NHS were quenched by 0.5 ml, 10 mM glycine containing phosphate buffer, pH 7.4, and kept at room temperature for 30 minutes with continuous end-to-end mixing. After quenching, the nanoconjugates Cur_Tpt_NC.MB (Fig. 1C) were ready for further analysis. Likewise, blank nanoconjugates NC_B.MB were also developed, but in their case nanocapsules were not loaded with drugs. The nanoconjugates NC-FITC.MB-ND were developed by the same method, except Cur_Tpt_NC was replaced with NC-FITC and MB with MB-ND. Also, the Rh6g-loaded nanoconjugates NC-Rh6g.MB were prepared by the same method, though NC-Rh6g was substituted for Cur_Tpt_NC.

Characterization of Nanoconjugates Cur_Tpt_NC.MB. The covalent nanoconjugates NC_B.MB developed from NC_B and MB through EDC-NHS coupling were analyzed by Fourier-transform infrared (FTIR) spectroscopy (3000 Hyperion Microscope with Vertex 80 FTIR system; Bruker) within a range of 400–4000 cm^{-1} using KBr pellets. But to avoid the false positive results in FTIR analysis, glycine PBS buffer was not added at the end to quench the EDC and NHS. To quantify the efficiency of coupling reaction, MB-ND (0.15 mg/ml of Nile red) and NC-FITC (1.2 mg/ml of FITC) were coupled by EDC-NHS reaction and then the amount of total nanoconjugates NC-FITC.MB.ND present in the reaction mixture was quantified by flow cytometry (BD FACS Aria; Becton, Dickinson and Company) through measurement of fluorescence intensity using PI-A (for Nile red) and FITC-A (for FITC) filters. The coupling reaction was also proved by determining hydrodynamic diameter, zeta potential, and morphology through cryo–field emission gun–scanning electron microscopy analysis. Nanoconjugates were also analyzed for the amount of drug retained after conjugation reaction.

Release Kinetics through Ultrasound Pulses. Cur_Tpt_NC and Cur_Tpt_NC.MB were transferred to a dialysis bag at a concentration such that both the conjugates had 2 and 1 mg/ml of Cur and Tpt, respectively, and then at times $t = 0$, 55, 115, and 175 minutes of release profile, study nanoconjugates were exposed to ultrasound at an intensity of 2 W/cm^2 for 60 and 15 seconds at 50% duty cycle. At time points 0, 30, 55, 60, 115, 120, 175, 180, and 210 minutes of the study, sampling was done as reported previously (Chandan and Banerjee, 2018). The amount of released drug was estimated by HPLC.

Preparation of Agarose Phantom Model and Echogenicity Measurement of MB and Tpt_NC.MB. Echogenicity of both MB and Cur_Tpt_NC.MB was elucidated in an agarose phantom model (Supplemental Fig. S3). One percent agarose was dissolved in degassed MQ at 80°C and then it was poured in a cuboidal open-end small acrylic casting tray. To create wells of 1-ml volume, the open end of the casting tray was covered with a three-dimensional printed (Ultimaker^2 3D printer; Graphite software) lid with spikes on one face, and the whole tray was kept at 4°C for 1 hour. After 1 hour, the tray was taken out and the lid was then removed to generate wells. Finally, a solidified agarose block was removed carefully from the tray (Supplemental Fig. S3). One milliliter of degassed PBS, SonoVue, MB, and Cur_Tpt_NC.MB equivalent to 5 mg/ml of lipid was added to each well, and then B-mode imaging was performed using a sonography instrument (LOGIC P9; GE Healthcare) at parameters of mechanical index 1–1.2, frequency 10 MHz, and thermal index for soft tissue (TIs) 0.4. An ultrasound probe (9L-D; GE healthcare) was placed at angle of 90° to the depth of the well. Distance between well and ultrasound probe was 3 cm.

Cell Culture. M. D. Anderson metastatic breast cancer cell (MDA MB 231) and B16F10 murine melanoma cells (B16F10) were cultured in DMEM supplemented with 10% FBS and 1% antibiotic antimycotic solution and maintained in humidified environment of 5% CO_2 at 37°C. In 24-well plates, cells were seeded 1×10^5 cells per well, and 3×10^4 in 96-well plates. In all cases, cell viability was determined by MTT assay (Mosmann, 1983). In brief, the culture medium of each well was replaced with 200 μl of MTT solution (0.05% of MTT dissolved in Hank's balance salt solution) MTT led to the formation of formazan crystals inside the cells, which were dissolved by a reagent composed of 10% Triton X-100 and 0.1 N HCl in anhydrous isopropyl alcohol. After complete dissolution of the crystals, absorbance was measured at 590 nm, and the baseline was corrected by measuring absorbance at 620 nm. Cells were procured from the National Centre for Cell Sciences, Pune, India.

MB and Sonoporation. Cells were seeded in 96-well plates 3×10^3 cells per well and allowed to grow for 24 hours to reach 90% confluence. Wells were then decanted and replaced with fresh DMEM culture medium containing 150 μg of MB. This was followed by treatment with ultrasound at an intensity of 2 W/cm^2, 50% duty cycle, for 15 seconds. Just after treatment cells were fixed with 10% formaldehyde containing PBS and incubated for 10 minutes. Thereafter, cells were frozen in liquid nitrogen and then sublimed at −90°C for 10 minutes. The sublimed cells were then coated with platinum at 10 mA for 60 seconds and then analyzed by scanning electron microscopy.

Cellular Internalization. To study the cellular internalization, MDA MB 231 cells seeded 1×10^5 cells/well were allowed to grow until 90% confluent in 24-well plates, and then medium was decanted and fresh medium added containing10 μg of Rh6g encapsulated inside NC-Rh6g and NC-Rh6g.MB. Just after addition, cells were treated with ultrasound (SONIDEL SP100) at 50% duty cycle and 0.9 W/cm^2 intensity for 15 seconds. After 1.5 hours of incubation, culture medium was discarded and cells were washed twice with ice-cold PBS, then fixed with ice-cold 10% formaldehyde solution prepared in PBS, and observed through a confocal laser scanning microscope (CLSM; Olympus Fluoview, FV500; Tokyo, Japan) at excitation and emission wavelengths of 525 and 548 nm, respectively, for Rh6g, and images were obtained at 60× through oil immersion objective using the Fluoview software (Olympus). For single-cell analysis by flow cytometry, cells were washed twice with PBS (temperature 37°C) and then 300 μl of trypsin-EDTA was added. After 2–3 minutes of incubation, 300 μl of DMEM was added to neutralize the trypsin, and cells were isolated through centrifugation at 3000*g* for 2 minutes. Isolated cells were resuspended in 500 μl of 1% formaldehyde and analyzed by flow cytometry using a PE-A filter for fluorescence intensity of Rh6g/NC-Rh6g internalized by the cells.

In Vitro Cytotoxicity. MDA MB 231 and B16F10 cells were allowed to grow for 24 hours in 96-well plates, and then wells were decanted and filled with Tpt, Tpt_NC, and Tpt_NC.MB, containing culture medium with the Tpt concentrations 50, 12.5, 3.1, 0.8, 0.2, 0.04, and 0.01 μM. After addition of Tpt_NC.MB, cells were treated with ultrasound at 0.9, 1.5, 2, and 2.5 W/cm^2 intensity at 50% duty cycle for 15 seconds by placing the culture plate over the ultrasound probe (SONIDEL SP100). A thin layer of gel (Kiran sonogel) was placed between the plate and probe to prevent the air attenuation of the ultrasound. To determine the cytotoxicity of Cur in the presence of ultrasound, 100, 25, 6.3, 1.6, 0.4, 0.1, and 0.02 μM concentrations of free and encapsulated Cur, such as Cur_NC, Cur_NC.MB, were incubated with the cells, and just after that ultrasound was applied. In free-drug treatment, Cur and Tpt were dissolved in dimethyl sulfoxide at a concentration of 20 mg/ml and were further diluted in DMEM to obtain the required concentration. To determine the combination index, the physical mixture of two drugs and drugs coencapsulated inside nanoconjugates, Cur_Tpt_NC.MB, were incubated with two cell lines at the same concentration as was used earlier to determine cytotoxicity. Ultrasound treatment was given at same parameters. The concentration of Cur and Tpt was used uniformly in all the treatments. After treatment with ultrasound, cells were incubated for 72 hours and thereafter cell viability was determined by MTT assay.

Apoptosis Assay. To test apoptotic induction ability, MDA MB 231 cells were seeded in 24-well plates, allowed to grow until 90% confluent, and then treated with Tpt, Tpt_NC, Tpt_NC.MB, and Tpt_NC.MB+US2 at a concentration of 70 nM (IC_{50} concentration of Tpt_NC.MB+US2). Likewise for Cur, cells were treated with 220 nM

Downloaded from jpet.aspetjournals.org at ASPET Journals on April 10, 2024

Cur (IC_{50} concentration of Cur_NC.MB+US2), Cur_NC, Cur_NC.MB, and Cur_NC.MB+US2. In dual-drug treatment, cells were treated with 50 nM Tpt and 100 nM Cur (IC_{50} concentration of Cur_Tpt_NC.MB+US2) as Cur-free, Tpt-free, Cur+Tpt–free physical mixture, Cur_NC.MB+US2, Tpt_NC.MB+US2, and Cur_Tpt_NC.MB+US2. After 72 hours' incubation, cells were isolated through trypsinization and washed with ice-cold washing buffer (0.1% azide + 5% FBS in PBS) before resuspension in 500 μl of ice-cold binding buffer [10 mM 4-(2-hydroxyethyl) piperazine-1-ethanesulphonic acid + 150 mM NaCl + 5 mM KCl + 1 mM $MgCl_2$ + 1.8 mM $CaCl_2$ at pH 7.4]. After 5–10 minutes' incubation in binding buffer, 3 μl of annexin-V FITC (Invitrogen, ThermoFisher Scientific) was added to each tube and incubated for 45–60 minutes in ice-cold condition. Fifteen to 20 minutes before analysis 2.5 μg of PI was added. The population of necrotic cells, live cells, and early apoptotic and late apoptotic cells were differentiated by flow cytometry.

In Vivo Pharmacokinetic Study. Approval from an ethics committee organized by Apt Testing and Research Pvt. Ltd, Pune, was obtained before commencement of all types of in vivo study and no inhumane means were used to treat the animals. To study the plasma concentration of drugs over the period of time, 10 and 5 mg/kg of body weight doses of Cur and Tpt in free form and encapsulated inside Cur_Tpt_NC.MB were administered through the tail vein in female Wistar rats (n = 6, 6–8 weeks old, 200–250 g of body weight). A single dose of formulation was administered, and at 0, 1, 2, 6, 8, 10, and 24 hours postinjection 0.5 ml blood samples were collected by retro-orbital puncture and stored at −20°C for 8–10 hours before estimation. The amount of Cur and Tpt in plasma was coestimated by HPLC (Vareed et al., 2008; Tiwari et al., 2014). Briefly, 100 μl of plasma was mixed with 25 μl of β-glucuronidase (500 IU) in 0.1 M phosphate buffer (pH 6.8) and incubated for 3.5 hours at 37°C, as reported by Vareed et al. (2008). Thereafter, the whole mixture was precipitated by addition of 1 ml of an ice-cold mixture of ethyl acetate and methanol (95:5, v/v) with strong agitation. The precipitated mixture was then centrifuged at 10,000g for 15 minutes at 4°C. Uppermost separated solvent layer was then isolated and the process was repeated thrice to isolate the maximum amount of Cur and Tpt. The collected solvent mixture was then evaporated under a stream of nitrogen vapor and reconstituted in 0.5 ml of mobile-phase comprised acetonitrile, methanol and 20 mM acetate buffer with pH 3 (40:30:30, v/v). Twenty microliters of extract was injected and the mobile phase was pumped through the column (RP-18, 5 μm; LiChrosorb Merck) with a flow rate of 1 ml/min. The photodiode array detector was set at 420 and 228 nm for Cur and Tpt, respectively. The amount of drug in plasma was quantified by standard curve interpolation method through drug-spiking in blank plasma with a concentration range of 0, 1, 2, 3, 4, 5, 6, and 7 μg/ml of Cur and Tpt. For estimating the amount of Cur and Tpt in vital organs, each organ was weighed and then 0.5 g of the organs, including liver, kidney, spleen, lung, brain, Peyer's patch, and heart, was homogenized in 2 ml of 0.5 M acetate buffer (pH 5). Three milliliters of ice-cold ethyl acetate and methanol (95:5, v/v) was added and agitated for 5 minutes to precipitate the whole extract. The remainder of the process was similar to the extraction of drugs from plasma. Tissues were extracted thrice to isolate the maximum amount of drug.

In Vivo Antitumor Efficacy. Maximum tolerated dose (MTD) of the drug in mice was determined by administering (intravenously through tail vein) a higher amount of drug and then gradually decreasing the concentration. The MTD study was conducted for the C57BL/6 mice (n = 3, body weight 22–25 g) at concentrations of 20 and 10, 10 and 5, and 5 and 2.5 mg/kg of body weight of Cur and Tpt, respectively. After injection physiologic behavior of the animals was monitored.

To determine the antitumor efficacy of the formulation, a subcutaneous B16F10 melanoma tumor model was generated on both right and left flanks of the C57BL/6 mice (body weight 22–25 g, n = 6) by an injection of 2×10^6 cells/0.2 ml s.c. on both the flanks. The growth of the tumor was monitored, and after 15 days the tumor volume had reached up to 50–100 mm^3 and treatment was started. The first three treatments were given on alternate days and thereafter two treatments were given keeping a gap of 2 days. The dose of administered drug (intravenously through tail vein) was 5 and 2.5 mg/kg of body weight for Cur and Tpt, respectively. Just after injection, the ultrasound treatment was given to the right tumor at parameters of 2 W/cm^2, 50% duty cycle, for 60 seconds, and the left tumor remained unexposed. Tumor size was taken with a Vernier caliper for 15 days after initiation of treatment, and tumor volume was calculated using formula:

$$Tumor\ volume = \frac{W^2 \times L}{2}$$

where W is width of the tumor and L is length of the tumor.

To demonstrate the spatiotemporal delivery of dye in the presence of ultrasound, another experiment was performed in which NC-Rh6g.MB (dose: 10 mg/kg of body weight) was administered intravenously through the tail vein and just after that the right tumor was exposed to ultrasound at 2 W/cm^2 intensity and 50% duty cycle for 60 seconds. Thereafter, tumors were excised and fixed in 2.5% glutaraldehyde solution. The fixed tissue samples were then dehydrated by gradual multiple increased concentration of ethanol and cleared with xylene. Cleared tissues were now cast in molten wax. After the formation of wax block, 40- to 50-μm thick sections were prepared using a microtome and placed over a glass slide, which was kept in a hot air oven at 30–40°C for 15–20 minutes. Slides were then analyzed by CLSM at an excitation wavelength of 525 nm and emission wavelength of 548 nm at 20× magnification.

Data Analysis. All the experiments were performed in triplicate unless stated otherwise. IC_{50} values were determined by GraphPad Prism 5, and all flow cytometry data were analyzed by FCS Express 5. Data are presented in the form of mean ± S.D. and P value was calculated by Student's t test (two-tailed). Error bars represent the positive and negative S.D. from the mean value.

Results

Preparation and Characterization of Cur_Tpt_NC and MB. Cur_NE and Cur_Tpt_NC were both prepared and characterized. A schematic of the nanocapsule and its preparation procedure is provided in Fig. 1. Different ratios of lecithin, Cur and chitosan, Tpt were used to optimize the hydrodynamic diameter, zeta potential, and encapsulation efficiency (EE) of Cur_Tpt_NC (Supplemental Table S1). The Cur_Tpt_NC with EE (%) of 35% ± 4.4% and 60.6% ± 4.3% for Tpt and Cur, respectively, was chosen for further study as it entrapped the maximum amount of drug and dispersed uniformly in MQ. The hydrodynamic diameters of the Cur_NE and the Cur_Tpt_NC were found to be 55.5 ± 7.2 and 170.9 ± 20.3 nm, respectively (Fig. 2I.A). The chitosan coating over Cur_ NE increased its size and resulted into a core-shell bearing nanocapsule Cur_Tpt_NC. Electron microscopic examination had reconfirmed the size of both particles and also depicted the internal features and topology of the Cur_NE (Fig. 2II.A) and the Cur_Tpt_NC (Fig. 2II.B). Zeta potential of Cur_NE was −35.6 ± 9.5 mV and coating of chitosan completely reversed the same to 23.3 ± 5.7 mV. Reversal of zeta potential occurred owing to the coating of positively charged chitosan over the Cur_NE. Hydrodynamic diameter and zeta potential of MB were found to be 1200.6 ± 201.8 nm (Fig. 2I.C) and −15.9 ± 4.8 mV, respectively. Electron microscopic imaging illustrated its spherical shape and reconfirmed the size obtained through DLS (Fig. 2II.C). The EE (%) of dye in NC-FITC, NC-Rh6g, and MB-ND was found to be 60% ± 10%, 62.7% ± 3%, and 75% ± 5%, respectively.

Downloaded from jpet.aspetjournals.org at ASPET Journals on April 10, 2024

TABLE 1
Increase in forward scatter and side scatter after conjugation of nanoparticles

Nanoparticles	FSC	SSC
NC-FITC[a]	1540 ± 114	1302.3 ± 170
MB-ND[b]	1675 ± 112.9	1268.3 ± 140.7
NC-FITC.MB-ND[c]	3080 ± 136.5	3842 ± 178

FSC, Forward scatter; SSC, side scatter.
[a]FITC-stained chitosan nanocapsules.
[b]Nile red-stained microbubbles.
[c]Covalently linked MB-ND and NC-FITC.

TABLE 2
Molar ratio of EDC.HCl/NHS and corresponding percentages of conjugates (Cur_Tpt_NC.MB) formed after coupling reaction

EDC.HCl/NHS (mM)	Percentage of Nanoconjugates (Cur_Tpt_NC.MB)
1:2	84.6 ± 5.56
1:3	80.4 ± 4.47

Characterization of Nanoconjugates Cur_Tpt_NC.MB. Cur_Tpt_NC and MB were conjugated through formation of amide linkage. In FTIR spectroscopic analysis, an intense new peak was obtained in the spectrum of nanoconjugate NC_B.MB at 1417 cm^{-1} (Fig. 3II.A, shown inside rectangle) that was not present initially in blank nanocapsule and MB. This new peak confirmed the synthesis of new C–N bond (shown in red, Fig. 3II.C) between chitosan of NC_B and DOPS of MB. This new peak at 1417 cm^{-1} appeared to result from stretching vibration of newly developed C–N amide bond. Likewise, other peaks that are evidence of formation of amide bonds are at 1577 cm^{-1} in NC_B.MB owing to NH-amide bending and at 1647 cm^{-1} in the NC_B.MB spectrum resulting from vibration stretching the carbonyl group of the amide bond (Morelli et al., 2011; Jain et al., 2012; Wang et al., 2016). To quantify the efficiency of conjugation reaction, the MB-ND and NC-FITC were linked together by amide linkage, and flow cytometry assay was performed to assess the amount of covalently linked nanoconjugates NC-FITC.MB-ND out of the total existing population, including MB-ND, NC-FITC, and NC-FITC.MB-ND. In flow cytometry analysis, MB-ND occupied quadrant Q4 (Fig. 3I.A) and NC-FITC occupied quadrants Q1 and Q3 (Fig. 3I.B). Therefore, nanoconjugates NC-FITC.MB-ND occupied quadrant Q2 as it comprised both MB-ND and NC-FITC (Fig. 3I.C). Other parameters correspond to changes in the size of the analyte are forward scatter (FSC-A) and side scatter (SSC-A). The values of both SSC-A and FSC-A were enhanced by 2- and 3-fold, respectively, which was evidence of the increase in size attributable to conjugation of NC-FITC and MB-ND (Table 1). Gottstein et al. (2013) demonstrated the same concept and reported the increase in FSC-A and SSC-A values upon aggregation of nanoparticles. Concentrations of EDC/NHS in 1:2 and 1:3 molar ratios provided conjugated populations of 84.6% ± 5.6% and 80.4% ± 4.5%, respectively, as shown in Table 2. We carried out the remainder of the study using a 1:2 molar ratio, as it had provided the maximum population of NC-FITC.MB-ND. The nanoconjugates are dual-nanoparticle systems with small nanometer size (Cur_Tpt_NC adsorbed over MB is the central micrometer-sized particle) (Fig. 2II.D–F). The hydrodynamic diameter of the developed nanoconjugate was 1760.4 ± 350.3 nm (Supplemental Fig. S2), which is in agreement of with the diameter obtained from field emission gun–scanning electron microscopy analysis. The zeta potential of nanoconjugates was found to be −12.7 ± 2.3 mV (Supplemental Table S1). The EE percentages of Cur and Tpt inside Cur_Tpt_NC.MB were found to be 33.1% ± 2.3% and 58.32% ± 2.9%, respectively (Supplemental Table S1).

Release Kinetics through Ultrasound Pulses. The nanoconjugates and nanocapsules were treated with ultrasound stimulus, and the effect of ultrasound on release of drug from carrier was observed. It was found that stimulus enhanced the release of drug from nanocarriers. Exposure with ultrasound released 28.9% ± 2.1% of Cur from Cur_Tpt_NC.MB within 3.5 hours and 43% ± 4.5% of Tpt within the same time after three insonations of 60 seconds at 1-hour intervals, whereas in the absence of ultrasound stimulus, the same amount of nanoconjugates released just 7% ± 3.1% and 14% ± 2.9% of Cur and Tpt within same period. In the case of a 15-second exposure with ultrasound, 12% ± 2.3% of Cur and 24.29% ± 3.24% of Tpt were released from the nanoconjugates, which was higher than the drug released in the nonstimulus condition but lower than that for the 60-second exposure time. Although ultrasound exposure did enhance the release of drug from nanocapsules Cur_Tpt_NC, even in the absence of MB, but the degree of enhancement was lower than when MB was conjugated to nanocapsules (Fig. 4).

Echogenicity of MB and Cur_Tpt_NC.MB in an Agarose Phantom Model. A B-mode image was captured. Both MB and Cur_Tpt_NC.MB showed ultrasound contrast. A small bright circular area can be seen against the dark background in the B-mode image (Fig. 5I). Both Cur_Tpt_NC.MB and MB had shown that ultrasound contrast and pixel intensity of the image were similar to that of an image obtained from commercialized SonoVue (Fig. 5I.E). Degassed PBS used as control showed hardly any contrast against the background.

MB and Ultrasound Induced Sonoporation in MDA MB 231 and B16F10 Cells. The study was done to observe the effect of insonation on cells in the presence and absence of MB. The number and diameter of the pores obtained through a sole ultrasound treatment over MDA MB 231 cells was limited to one to two pores/cell of 220 nm (Fig. 5II.B, black dotted circle), but in the presence of MB, ultrasound exposure increased the number to 6–8 pores/cells (Fig. 5II.C) and also increased the diameters of a few pores to 400–600 nm (Fig. 5II.C, black dotted circle), whereas others were relatively smaller in diameter (Fig. 5II.C, white dotted circle).

The experiment was repeated in B16F10 melanoma cells, and similar results were observed in terms of diameter and number of pores generated in plasma membrane (Fig. 5II.D–F). Therefore, it is now evident that the presence of MB in the culture medium increases the diameter as well as the number of sonopores per cell two to three times greater than in cells treated with ultrasound solely. The trend of sonoporation, i.e., number of pores/cell with ultrasound exposure in presence and absence of MB, is shown in Fig. 6.

Cellular Internalization Study. The effect of MB-assisted ultrasound treatment on internalization of nanoparticles was studied by both CLSM and flow cytometry. CLSM images of MDA MB 231 cells showed enhanced cellular internalization on application of ultrasound (Fig. 7I.(a).D) compared with the controls (Fig. 7I.(a).A–C). The pixel intensity of the red fluorescent cells was plotted for all four images, is summarized in Fig. 7I.(b), and showed that the ultrasound application enhanced the fluorescence intensity of cells by

Downloaded from jpet.aspetjournals.org at ASPET Journals on April 10, 2024

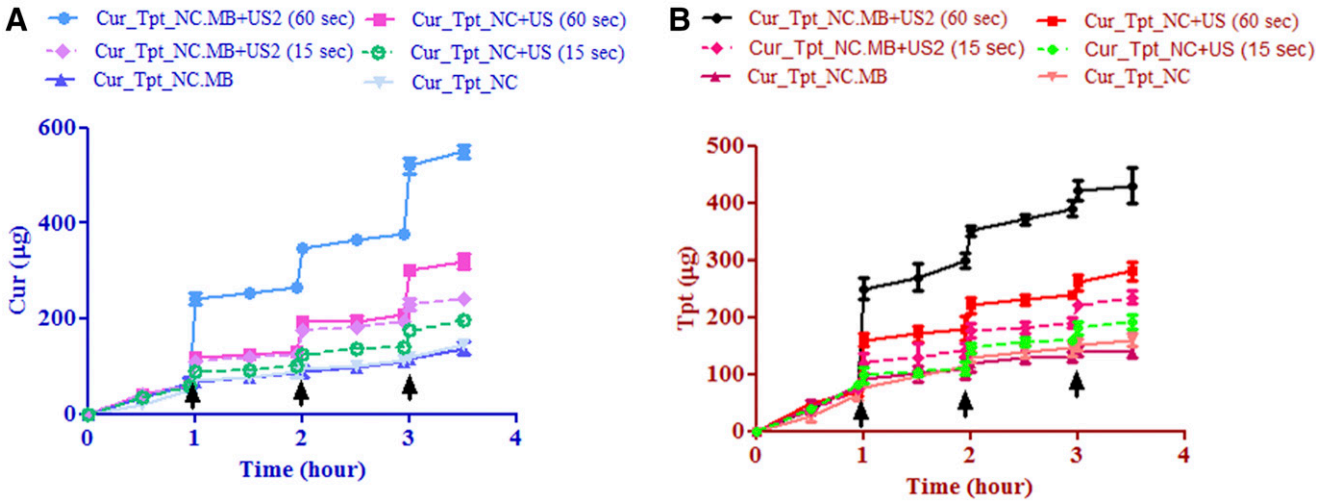

Fig. 4. Release kinetics of (A) Cur and (B) Tpt from Cur_Tpt_NC and Cur_Tpt_NC.MB in presence of ultrasound exposure at 2 W/cm^2 at 50% duty cycle for 15 and 60 seconds. Arrows show time at which ultrasound exposure was given.

2.5–3 times owing to higher internalization compared with unexposed cells. In another experiment, the degree of enhancement was quantified by flow cytometry, and fluorescence intensity was found to have increased gradually with the increase in ultrasound intensity from 0.8 to 1.1 W/cm^2 at 50% duty cycle and 15-second exposure time (Fig. 7II). The fluorescence intensity inside cells is the measure of the amount of internalized rhodamine 6g contained in nanoconjugates NC-Rh6g.MB and nanocapsules NC-Rh6g. Single-cell quantification by flow cytometry gave the fluorescence intensities of 3480 ± 498.7, 5427 ± 354.3, 5930 ± 395.7, and 6470 ± 639.2 (Fig. 7II) at ultrasound intensities 0.8, 0.9, 1, and 1.1 W/cm^2, respectively. On the other hand, in negative controls, in which NC-Rh6g.MB and NC-Rh6g were simply incubated with cells without any ultrasound treatment, fluorescence intensities were found to be as low as 1656.3 ± 160.5 and 2083 ± 307.6, respectively (Fig. 7II). These results showed that the insonation increased the cellular internalization 2- to 4-fold compared with negative control, and this was in agreement with the CLSM analysis of the Rh6g-internalized cells. In flow cytometry assay, it was found that insonation not only enhanced the cellular internalization but also increased the population of cells positive for Rh6g. Only 32.7% (Fig. 7III, B and E) of the population internalized the encapsulated dye in the absence of ultrasound, but the exposure to ultrasound in the presence of NC-Rh6g.MB increased the population of Rh6g-positive cells by up to 89.4% (Fig. 7III, C and F). In CLSM analysis also, a few cells lacked fluorescence at all (Fig. 7I(a).B, green arrow) or had very low fluorescence (Fig. 7I(a).C, green arrow) in the absence of ultrasound exposure, but insonation made the cells positive for Rh6g uniformly (Fig. 7I.(a).D) with very high intensity.

In Vitro Cytotoxicity. The concentration of drug at which 50% of the exiting population of cells was dead, the IC_{50} value, was determined for both free and encapsulated drug in the presence of ultrasound in MDA MB 231 and B16F10 cells (Fig. 8) and summarized in Table 3. When ultrasound was applied on MDA MB 231 cells in the presence of Cur_Tpt_NC.MB, the IC_{50}s of Tpt and Cur were reduced to 0.04 ± 0.011 and 0.08 ± 0.010 μM, respectively (combination index: 0.93; Table 3), which are 112 and 265 times lower than the IC_{50} concentrations of free Tpt and Cur, respectively (Fig. 8A). Also, in B16F10 cells, after ultrasound exposure in the presence of Cur_Tpt_NC.MB, the IC_{50} concentrations of Tpt and Cur were 0.06 ± 0.019 and 0.11 ± 0.01 μM, respectively (combination index: 0.85), which are 100 and 150 times lower than the IC_{50} concentrations of free Tpt and Cur, respectively, (Fig. 8B; Table 3). Although the combination index values in both cells does not indicate a tendency toward strong synergism between Tpt and Cur, it does indicate an additive effect. In addition, the increase in intensity of ultrasound at constant duty cycle and exposure time increased the cytotoxicity of both Tpt_NC.MB and Cur_NC.MB at intensities of 0.9, 1.5, 2, and 2.5 W/cm^2, as shown in Fig. 8, C and D. However, a further increase in intensity was not considered, as even blank nanoconjugates NC_B.MB were causing very high cytotoxicity at 2.5 and 3 W/cm^2, and maximum cell viability was found to be 80% and 45%, respectively, at the lowest concentration of NC_B.MB (0.007 μg/ml, MB), whereas ≥90% of MDA MB 231 cells were viable at 2 W/cm^2 (Supplemental Fig. S4). In contrast, in the absence of MB and drug, ultrasound was nontoxic at intensities of 0.9, 1.5, 2, and 2.5 W/cm^2 with fixed duty cycle of 50% and exposure time of 15 seconds (Supplemental Fig. S5).

Apoptosis Assay. Ultrasound exposure increased the sum of necrotic and apoptotic cells significantly compared with free drugs and their physical mixture (Fig. 9) (detailed results of the assay provided in Supplemental Fig. S6, S7 and S8). Treatment with ultrasound, at an intensity of 2 W/cm^2, duty cycle 50%, for 15 seconds, significantly increased the sum of apoptotic and necrotic cells by 4.1 and 5.8 fold compared with Tpt and Tpt_NC.MB (Fig. 9A). Likewise, in the case of Cur, the enhancement occurred by 5.5- and 2.5-fold compared with Cur and Cur_NC.MB (Fig. 9A). In combinational treatment, the sum of apoptotic and necrotic cells increased significantly owing to ultrasound exposure and the additive effect of drugs (Fig. 9B). The sum of apoptotic and necrotic cells increased by 3.2-fold in Cur_Tpt_NC.MB+US2 treatment compared with a physical mixture of drugs (Fig. 9B). The apoptosis-inducing abilities of Tpt, Tpt_NC, and Tpt_NC.MB were not significantly different from each other, as the IC_{50} concentration of Tpt_NC.MB+US2 was quite low, and at this concentration the formulations including Tpt, Tpt_NC, and Tpt_NC.MB were yielding almost similar cytotoxicity.

Downloaded from jpet.aspetjournals.org at ASPET Journals on April 10, 2024

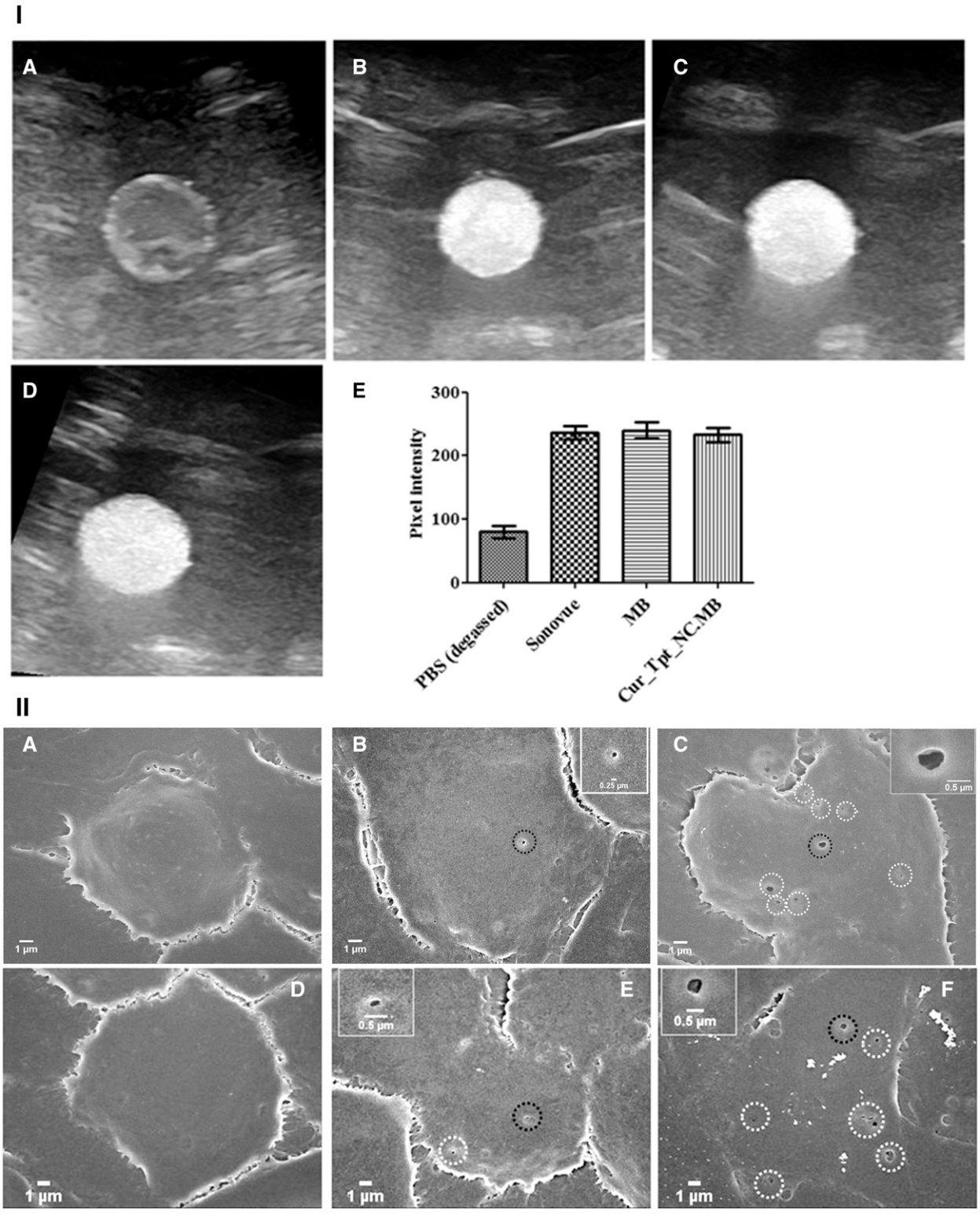

Fig. 5. I. Ultrasound contrast property of ultrasound contrast agents and comparison of pixel intensity. (A) Degassed PBS, (B) SonoVue, (C) MB, and (D) Cur_Tpt_NC.MB. (E) Comparison of pixel intensity of white spherical area. II. Effect of ultrasound on MDA MB 231cells in presence of MB: (A) no ultrasound treatment, (B) ultrasound treatment 2 W/cm^2, 50% duty cycle, for 15 seconds without MB; inset image shows magnified view of pore indicated by black dotted circle. Scale bar in inset is 0.25 μm. (C) Ultrasound treatment 2 W/cm^2, 50% duty cycle, for 15 seconds, with MB; inset image shows magnified view of pore indicated by black dotted circle. Black- and white- dotted circles denote sonopores. Scale bar in inset is 0.5 μm. In B16F10 melanoma cells (D–F), similar effects were observed. Reaction condition of (A–C) was similar to (D–F), respectively. (E) Pore circled by black dots is shown in inset and scale bar in inset is 0.5 μm. (F) Pore circled by black dots is shown in inset and scale bar in inset is 0.5 μm.

Downloaded from jpet.aspetjournals.org at ASPET Journals on April 10, 2024

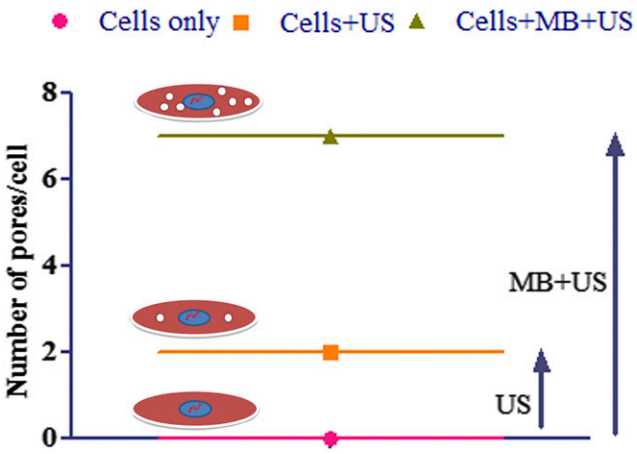

Fig. 6. Representation of the increase in number of pores/cell owing to ultrasound exposure (2 W/cm^2, 50% duty cycle, 15 seconds) in presence and absence of MB. White dots inside cells represent pores. US, ultrasound.

In Vivo Pharmacokinetic Study. All pharmacokinetic parameters were evaluated using noncompartmental analysis after the plasma concentrations of drugs were co-estimated using HPLC (Supplemental Fig. S9) over the period of time. The elimination half-lives ($T_{1/2}$) of free Cur and Tpt were 2.1 ± 0.3 and 2.3 ± 0.2 hours, but their encapsulation inside nanoconjugate Cur_Tpt_NC.MB increased the same to 11.5 ± 2.8 and 9.7 ± 1.6 hours, respectively. Encapsulation also increased the peak plasma concentration (C_{max}) of drugs from 8.8 ± 0.7 and 12.3 ± 0.8 μg to 28.6 ± 2.3 and 38.5 ± 3.5 μg for Cur and Tpt, respectively. Total drug exposure ($AUC_{0-\infty}$) for Cur and Tpt was 21.4 ± 1.2 and 27.6 ± 2.7 μg·h/ml, whereas their encapsulation inside nanoconjugates increased it up to 402.9 ± 5.3 and 424 ± 6.7 μg·h/ml, respectively. Not only the $AUC_{0-\infty}$, $T_{1/2}$, and C_{max}, but also the biodistribution of the drugs in vital organs increased (Supplemental Table S2) upon encapsulation inside nanoconjugates. Pharmacokinetic study showed that the encapsulation of both Cur and Tpt inside nanocapsules increased the $T_{1/2}$, C_{max}, $AUC_{0-\infty}$, and biodistribution of drug in various vital organs (Fig. 10; Table 4).

In Vivo Antitumor Efficacy. As proof of concept, Rh6g dye containing NC-Rh6g.MB was administered to mice, and thereafter ultrasound exposure to the right tumor enhanced the intratumoral internalization and thereby fluorescence intensity by 2.5-fold in both central as well as peripheral regions of right tumor (Fig. 11), compared to corresponding regions of the left tumor. This shows that a nanoconjugate can be a suitable carrier for spatiotemporal delivery of drug in the presence of ultrasound. As this combination of drug was not reported before in any literature, the MTD study was conducted as per the literature and clarified that more often mice may survive at the specific dose of an individual drug but may not survive if administered the same dose in combination with the same two or more drugs. Therefore, as 40 mg/kg of body weight of Cur was permissible in an oral dose in mice (in another oral delivery formulation, data not shown), for a combination of two drugs, 20 and 10 mg/kg of body weight (for Cur and Tpt, respectively) were chosen as the maximum doses for intravenous administration. In this study, MTD was determined totally on the basis of survival and external physiologic behavior of mice, and no toxicity profiling or histopathological study was done. An MTD study showed that the 5- and 2.5-mg/kg of body weight doses were nonlethal for all groups studied (Supplemental Table S3). Hence, this dose was chosen for our study. Tumor exposed to ultrasound showed faster reduction in tumor volume compared with the unexposed tumor in the same mouse. Also, the reduction in tumor volume occurred most pronouncedly in tumor treated with ultrasound in group Cur_Tpt_NC.MB and least in tumor not exposed to ultrasound in group Cur+Tpt free (Fig. 12, A and D). The relative growth rate was reduced significantly, by 12 times, in Cur_Tpt_NC.MB+US treatment compared with Cur+Tpt free+US on the 11th day (Fig. 12B). The Cur_Tpt_NC.MB+US treatment reduced the relative growth rate of tumor significantly, by 15-fold, compared with the Cur+Tpt free (Fig. 12C). Moreover, in the same group the ultrasound-exposed right tumor showed significantly reduced growth rate compared with the left tumor (not exposed with ultrasound), as observed in Cur_Tpt_NC.MB treatment (Fig. 12C). Also, in treatment groups Tpt_NC.MB, Cur_NC.MB, and Cur_Tpt_NC.MB, the relative growth of ultrasound-exposed right tumor was reduced 1.8-, 1.4-, and 4-fold more than the noninsonated left tumor in the same group (Fig. 12C). Owing to the additive effect of the drugs, the rate of tumor growth in treatment Cur_Tpt_NC.MB+US was significantly higher than both Tpt_NC.MB+US and Cur_NC.MB+US (Fig. 12C). Also, Kaplan-Meier survival analysis showed that 21.8% and 26.2% of the animals were alive in the saline and Cur+Tpt-free groups, whereas 93.7%, 78.7%, and 93.7% of the animals were alive at the end of treatment in groups Cur_NC.MB, Tpt_NC.MB, and Cur_Tpt_NC.MB (Fig. 12E). It is evident from the results that the encapsulation of the drugs inside nanoconjugates increased the antitumor efficacy and rate of survival at the same time. Body weight in every group of treatment increased in the later phase with very minimal downward deflection in initial phase of treatment (Fig. 12F).

Discussion

We developed and characterized the Cur and Tpt–coencapsulating Cur_Tpt_NC and MB. Thereafter, Cur_Tpt_NC and MB were conjugated and characterized by DLS, zeta-potentiometer, flow cytometry, and FTIR, which confirmed the synthesis of nanoconjugates Cur_Tpt_NC.MB. It is evident from the experimental results that both MB and Cur_Tpt_NC.MB have an ultrasound contrast property. The compression and rarefaction of MB and Cur_Tpt_NC.MB in the presence of ultrasound led to the generation of secondary harmonics, the basis of the ultrasonographic image (Fig. 5I) obtained in our agar phantom model study (Qin et al., 2009). MB and Cur_Tpt_NC.MB were proved to be efficient contrast agents, as their echogenicity was similar to the marketed formulation SonoVue.

Cavitation of MB in the presence of ultrasound generated secondary harmonics, and these secondary harmonics, as well as the primary incident ultrasound wave, developed shear stress around the cells and generated pores in the plasma membrane. Although the pores were also generated in cells after ultrasound exposure when MB was not added to the culture, those pores were of comparatively smaller diameter and fewer in number. This result showed that in the absence of MB the magnitude of developed shear force was smaller and that is why the pore diameter was small. But in the presence of MB, the shear stress developed was of higher magnitude

Downloaded from jpet.aspetjournals.org at ASPET Journals on April 10, 2024

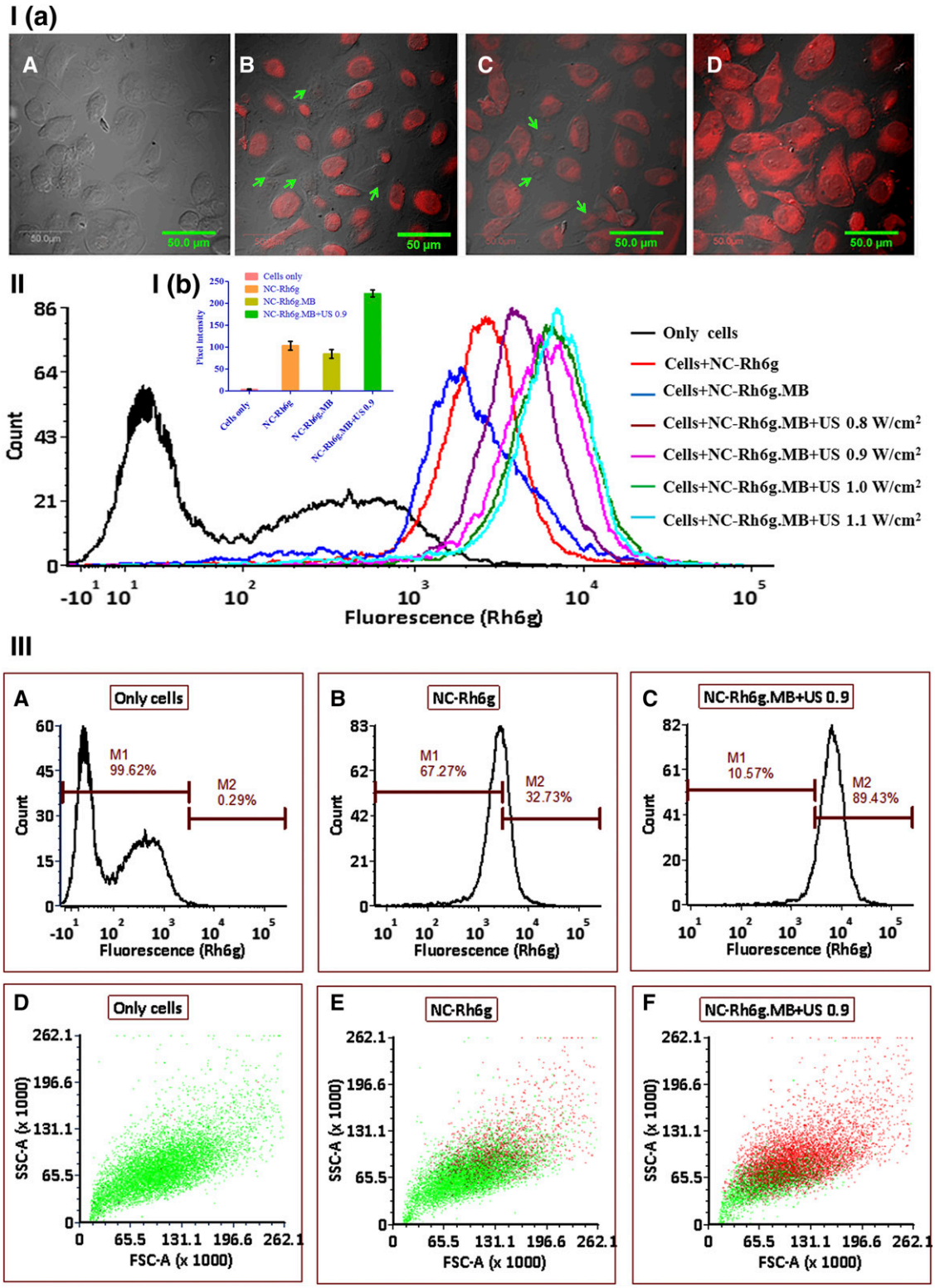

Fig. 7. I. (a) CLSM image shows internalization of NC-Rh6g and NC-Rh6g.MB in MDA MB 231 cells. (A) Only cells, (B) NC-Rh6g, (C) NC-Rh6g.MB, and (D) NC-Rh6g.MB + ultrasound (0.9 W/cm^2 intensity, 50% duty cycle and 15 seconds). Green arrow indicates cell without fluorescence or very minimal fluorescence. 1 (b) Comparison of the pixel intensity of red fluorescent area of I. (a) (A–D). II. Increase in amount of internalized rhodamine 6g inside cells with the increase in intensity of ultrasound from 0.8 to 1.1 W/cm^2. III. Increase in population of the MDA MB 231 cells involved in internalization. Green population (M1) indicates Rh6g negative cells, whereas red population (M2) indicates Rh6g positive cells. (A and D) Only cells; histogram of cell count vs. fluorescence intensity, M1: 99.6%. (B and E) NC-Rh6g-treated cell; histogram of cell count vs. fluorescence intensity, M2: 32.7% and M1: 67.3%. (C and F) NC-Rh6g.MB + Ultrasound (0.9 W/cm^2 intensity, 50% duty cycle and 15 seconds) –treated cells; histogram of cell count vs. fluorescence intensity, M2: 89.4% and M1: 10.6%.

Downloaded from jpet.aspetjournals.org at ASPET Journals on April 10, 2024

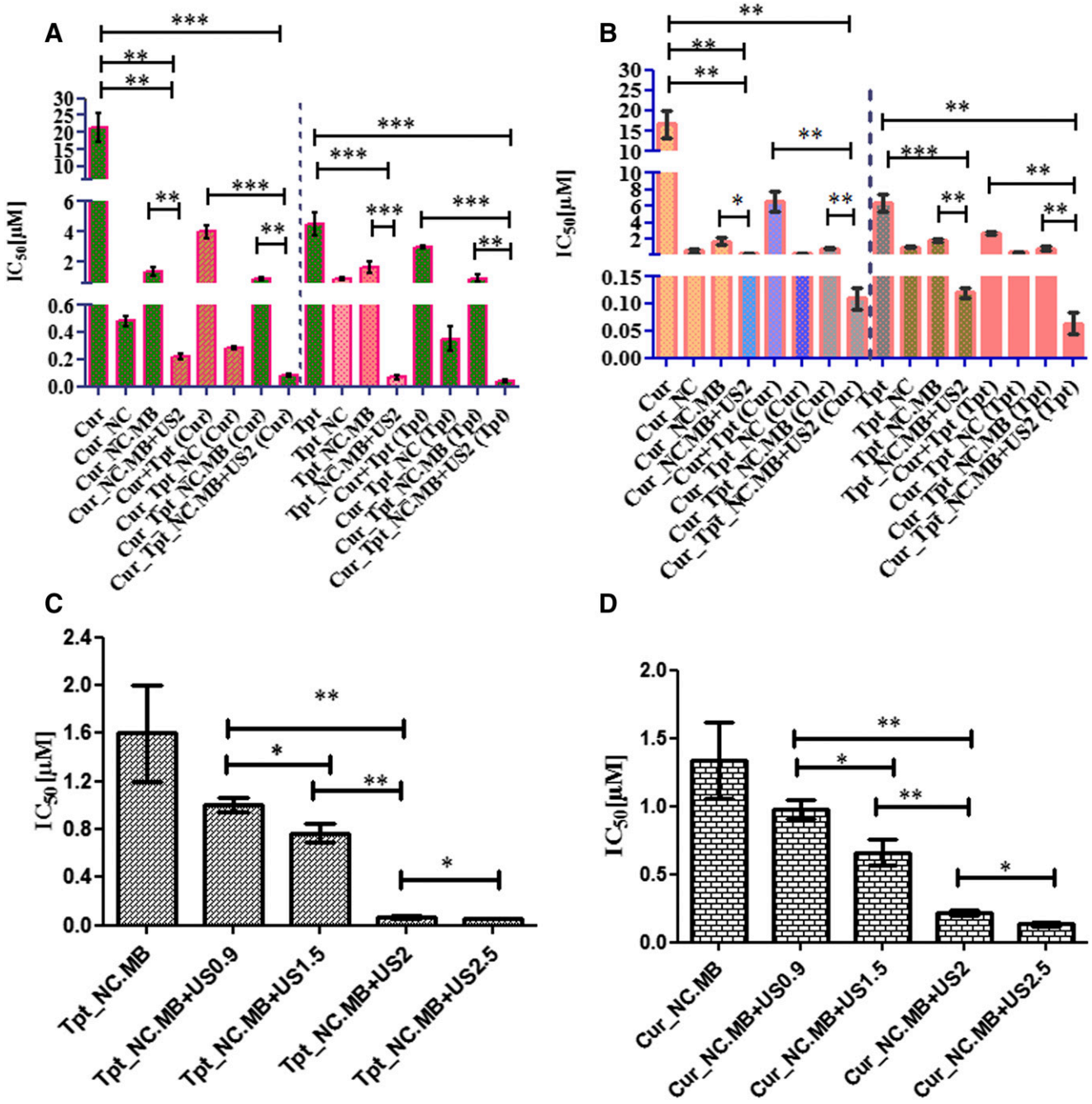

Fig. 8. (A) IC_{50} concentrations of formulations in MDA MB 231 cells. $^{**}P \leq 0.01$; $^{***}P \leq 0.001$. (B) IC_{50} concentrations of formulations in B16F10 melanoma cells. $^{*}P \leq 0.05$. $^{**}P \leq 0.01$; $^{***}P < 0.001$. (C) Decrease in IC_{50} with increase in intensity of ultrasound (0.9, 1.5, 2, and 2.5 W/cm^2) at fixed duty cycle (50%) and time period (15 seconds) in MDA MB 231 cells in presence of Tpt_NC.MB. $^{*}P \leq 0.05$; $^{**}P \leq 0.01$. (D) Decrease in IC_{50} with increase in intensity of ultrasound (0.9, 1.5, 2, and 2.5 W/cm^2) at fixed duty cycle (50%) and time period (15 seconds) in MDA MB 231 cells in presence of Cur_NC.MB. $^{*}P \leq 0.05$; $^{**}P \leq 0.01$ were calculated by Student's *t* test and data are represented as mean ± S.D. US0.9, ultrasound exposure at 50% duty cycle, 0.9 W/cm^2 intensity for 15 seconds; US1.5, ultrasound exposure at 50% duty cycle, 1.5 W/cm^2 intensity for 15 seconds; US2, ultrasound exposure at 50% duty cycle, 2 W/cm^2 intensity for 15 seconds; US2.5, ultrasound exposure at 50% duty cycle, 2.5 W/cm^2 intensity for 15 seconds.

owing to the cumulative action of the primary incident ultrasonic wave and the secondary harmonics. Consequently, the pores generated were of greater diameter as well as more numerous. Such sonopores in the plasma membrane, with increased diameter and number, would confer an additional advantage over the conventional cellular internalization of drug by increasing the intracellular drug concentration. However, the number of sonopores observed in SEM images (Fig. 5II.B, C, E, and F) of ultrasound-treated cells may not be representative of the exact number of pores generated by ultrasound exposure, as the process is transient and some of the pores could have resealed themselves before fixation. Therefore, the present result offers only a comparative insight into the effect of ultrasound on cells in the absence and presence of MB.

Application of ultrasound in the presence of MB would increase cellular internalization owing to the generation of sonopores. This is further proved by the study of the

Downloaded from jpet.aspetjournals.org at ASPET Journals on April 10, 2024

TABLE 3

IC_{50} concentration and combination index of the developed formulation in MDA MB 231 and B16F10 cells

Nanoparticle/Drug	MDA MB 231		B16F10	
Tpt	4.51 ± 0.75 μM	C.I. = 0.93	6.4 ± 0.98 μM	C.I. = 0.85
Cur+Tpt (Tpt)	3 ± 0.10 μM		2.8 ± 0.2 μM	
Tpt_NC	0.90 ± 0.03 μM		1.1 ± 0.08 μM	
Cur_Tpt_NC (Tpt)	0.35 ± 0.09 μM		0.43 ± 0.12 μM	
Tpt_NC.MB	5.75 ± 0.42 μM		1.89 ± 0.23 μM	
Tpt_NC.MB +US2	0.07 ± 0.013 μM		0.12 ± 0.01 μM	
Cur_Tpt_NC.MB (Tpt)	0.91 ± 0.23 μM		0.9 ± 0.23 μM	
Cur_Tpt_NC.MB+US2 (Tpt)	0.04 ± 0.011 μM		0.063 ± 0.02 μM	
Cur	21.25 ± 4.2 μM		16.67 ± 3.4 μM	
Cur+Tpt (Cur)	4 ± 0.40 μM		6.56 ± 1.2 μM	
Cur_NC	0.48 ± 0.04 μM		1.77 ± 0.45 μM	
Cur_Tpt_NC (Cur)	0.28 ± 0.01 μM		0.3 ± 0.03 μM	
Cur_NC.MB	1.34 ± 0.28 μM		1.77 ± 0.45 μM	
Cur_NC.MB+US2	0.22 ± 0.023 μM		0.33 ± 0.02 μM	
Cur_Tpt_NC.MB (Cur)	0.85 ± 0.1 μM		0.93 ± 0.1 μM	
Cur_Tpt_NC.MB+US2 (Cur)	0.08 ± 0.010 μM		0.11 ± 0.02 μM	

C.I., combination index.

internalization of NC-Rh6g.MB in the presence of ultrasound, and it was evident from the result that increased intracellular red fluorescence is attributable to the higher internalization of Rh6g in the form of NC-Rh6g.MB/NC-Rh6g/Rh6g through pores generated as a result of ultrasound exposure. Moreover, application of ultrasound in the presence of MB increased not only cellular internalization but also the number of cells participating in the process. Hence, ultrasound exposure could ensure effective regression of tumor by enabling maximum internalization of drug by a maximum number of the tumor's constituent cells. That is why the IC_{50} of Tpt_NC.MB+US2 and Cur_NC.MB+US2 in MDA MB 231 cells was reduced by 112- ad 265-fold compared with free Tpt and Cur, respectively (Table 3). Moreover, the additive effect of drugs could also contribute to a reduction in the IC_{50} of Cur_Tpt_NC.MB+US2; in the case of B16F10 melanoma cells, owing to the additive effect between drugs and the ultrasound exposure, IC_{50} concentration was reduced by 150- and 100-fold compared with free Cur and Tpt, respectively. When ultrasound was applied over cells in the presence of Tpt_NC.MB, Cur_NC.MB, and Cur_Tpt_NC.MB, inertial cavitation of these nanoconjugates led to the opening of cell membranes (Fig. 4II) and hence provided an opportunity for higher internalization of Tpt/Tpt_NC, Cur/Cur_NC, Cur_Tpt_NC/Cur/Tpt, indirectly compensating for the exocytic activity of P-glycoprotein receptors by ensuring adequate amount of drug inside the cells for effective inhibition of cancer cell proliferation.

The decrease in IC_{50} would have occurred as a result of other factors as well, for example, the encapsulation of Tpt and Cur inside Cur_Tpt_NC.MB. Encapsulation of Tpt inside

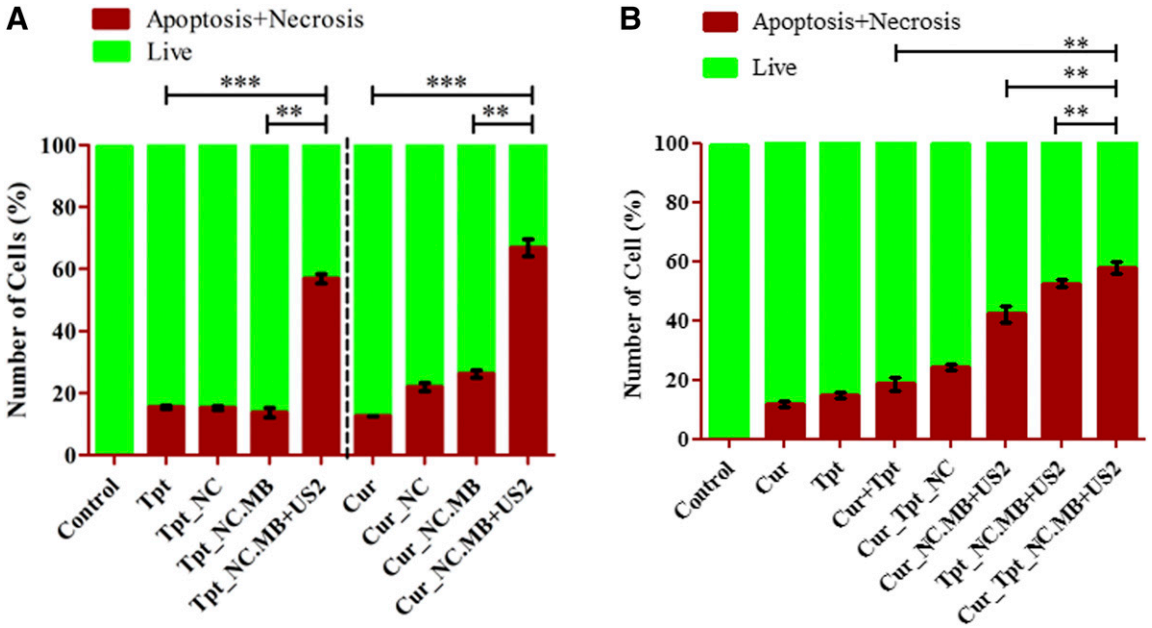

Fig. 9. Percentage population of apoptotic and necrotic cells in presence of: (A) Tpt, Tpt_NC, Tpt_NC.MB and Tpt_NC.MB+US2 at 70 nM concentration (IC_{50} concentration of Tpt_NC.MB+US2) and Cur, Cur_NC, Cur_NC.MB, Cur_NC.MB+US2 at 220 nM concentration (IC_{50} concentration of Cur_NC.MB+US2); (B) Cur, Tpt, Cur+Tpt, Cur_Tpt_NC, Cur_NC.MB+US2, Tpt_NC.MB+US2 and Cur_Tpt_NC.MB+US2 at 50 nM Tpt and 100 nM Cur. $^{**}P \leq 0.01$; $^{***}P \leq 0.001$. P value was calculated by Student's t test and data are presented as mean ± S.D.

Downloaded from jpet.aspetjournals.org at ASPET Journals on April 10, 2024

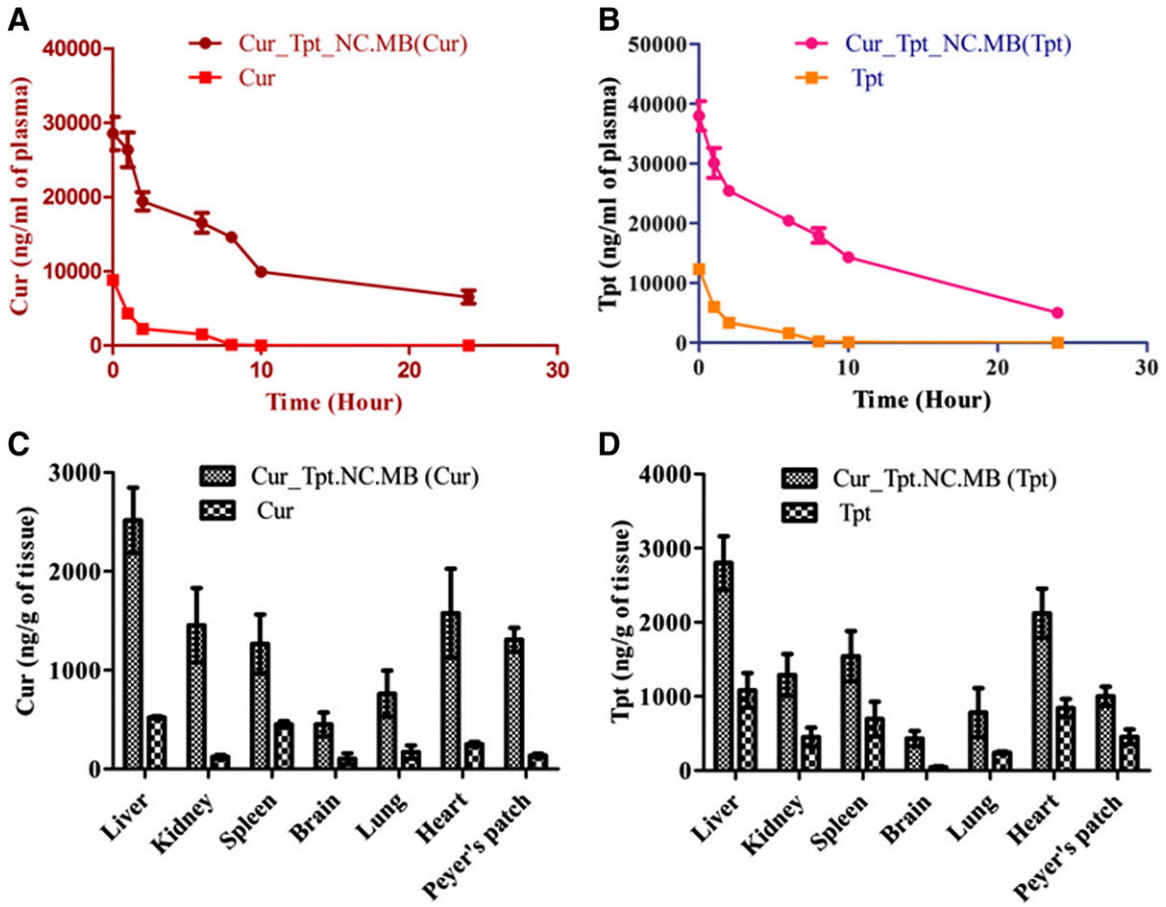

Fig. 10. Pharmacokinetic study of drugs when they were administered in both free and encapsulated form: (A) Cur, (B) Tpt. Cur, plasma concentration of Cur when free drug was administered; Cur_Tpt_NC.MB (Cur), plasma concentration of Cur when Cur_Tpt_NC.MB was administered; Cur_Tpt_NC.MB (Tpt), plasma concentration of Tpt when Cur_Tpt_NC.MB was administered; Tpt, plasma concentration of Tpt when free drug was administered. Biodistribution of drugs in vital organs: (C) Cur, (D) Tpt. Cur, Cur concentration in vital organs when free drug was administered; Cur_Tpt_NC.MB (Cur), Cur concentration in vital organs when Cur_Tpt_NC.MB was administered; Cur_Tpt_NC.MB (Tpt), Tpt concentration in vital organs when Cur_Tpt_NC.MB was administered; Tpt, Tpt concentration in vital organs when free drug was administered.

Cur_Tpt_NC prevented the Tpt from being exposed to the neutral or alkaline pH solution outside. Hence, Tpt did not ionize to carboxylate form and retained the cytotoxic efficacy that would have been compromised otherwise (Fassberg and Stella, 1992; Drummond et al., 2010). Likewise, the encapsulation of Cur inside Cur_Tpt_NC.MB would have increased the solubility of Cur, and thereby cellular internalization increased which in turn enhanced the cytotoxicity (Rao et al., 2014).

Moreover, intensity of ultrasound also played a crucial role in enhancing cytotoxicity of Tpt_NC.MB and Cur_NC.MB, as the cytotoxicity increased gradually with the increase in ultrasound intensity by 0.9, 1.5, 2, and 2.5 W/cm^2 (Fig. 8, C and D). Such an increase in cytotoxicity would have occurred because of the gradual increase in the magnitude of shear stress as the intensity of ultrasound increased in the presence of MB. This is in agreement with a previous report which stated, increased acoustic pressure decreased the cell viability in the presence of MB even at the same concentration of drug (Escoffre et al., 2013). However, in the absence of MB, the development of shear stress in culture medium would have been considerably lower and ≥95% cells would have remained viable at intensities of 0.9, 1.5, 2, and 2.5 W/cm^2, because MB is essential for amplifying the signal and generating secondary harmonics (Qin et al., 2009; Sirsi and Borden, 2012). Moreover, ultrasound exposure over MDA MB 231 breast cancer cells in presence of Cur_NC.MB, Tpt_NC.MB, and Cur_Tpt_NC.MB resulted in significant enhancement in the sum of apoptotic and necrotic cells compared with the effects of both individual drugs and their physical mixture (Fig. 9). Such an increase in the sum of apoptotic and necrotic cells upon ultrasound exposure in presence of drugs might have occurred because higher cellular internalization of drug would have in turn increased drug-induced apoptosis. Additionally, the shear stress created by ultrasound would have activated the intracellular signaling cascade that led to the apoptosis of cells. Although the exact mechanism of ultrasound-mediated apoptosis is still

TABLE 4
Pharmacokinetic study in Wistar rat shows enhancement in $T_{1/2}$ and C_{max} upon encapsulation inside nanoconjugate Cur_Tpt_NC.MB compared with free drug Tpt and Cur

Nanoparticles/Drug	$T_{1/2}$	C_{max}	$AUC_{0-\infty}$
	h	*μg*	*μg·h/ml*
Cur_Tpt_NC.MB(Tpt) I.V.	9.7 ± 1.6	38.5 ± 3.5	424 ± 6.7
Cur_Tpt_NC.MB(Cur) I.V.	11.5 ± 2.8	28.6 ± 2.3	402.9 ± 5.3
Tpt (I.V.)	2.3 ± 0.2	12.3 ± 0.8	27.6 ± 2.7
Cur (I.V.)	2.1 ± 0.3	8.8 ± 0.7	21.4 ± 1.2

Downloaded from jpet.aspetjournals.org at ASPET Journals on April 10, 2024

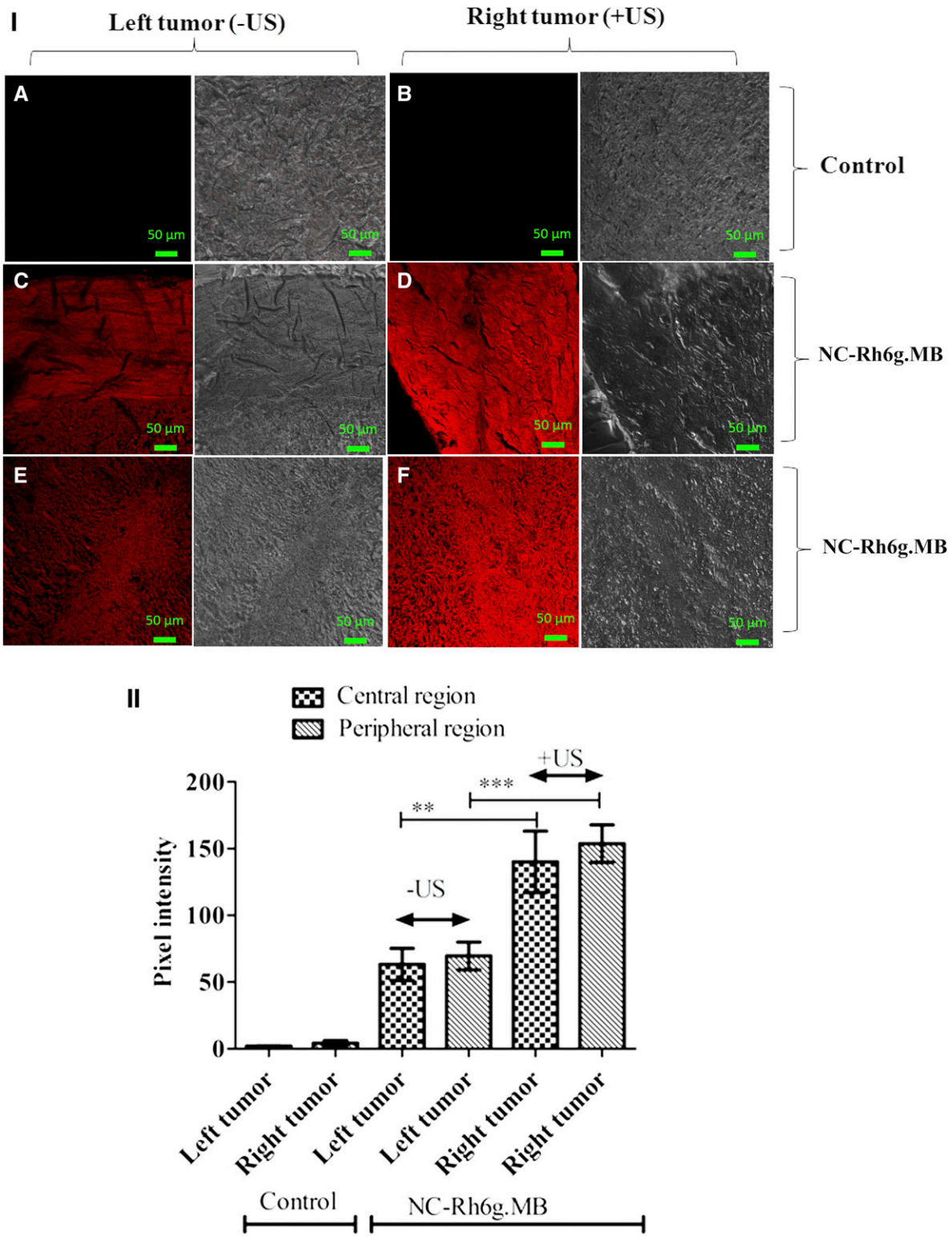

Fig. 11. CLSM images of the tumor tissue sections after intravenous injection of NC-Rh6g.MB followed with ultrasound exposure (2 W/cm^2, 50% duty cycle for 60 seconds). (A and B) control, (C and D) peripheral region of tumor, (E and F) central region of tumor. II. Ten points selected from image and their pixel intensities in terms of red fluorescence plotted for different regions and tumors. $^{**}P = 0.006$; $^{***}P = 0.001$.

unclear, only a few pathways have been suggested as being responsible (Feng et al., 2010; Li et al., 2012; Bohari et al., 2017). As far as the pharmacokinetic parameters are concerned, the increase in $AUC_{0-\infty}$, $T_{1/2}$, C_{max}, and biodistribution of both drugs is attributable to the encapsulation inside the nanoconjugate Cur_Tpt_NC.MB (Dobrovolskaia et al., 2008; Kurita and Makino, 2013; Petschauer et al., 2015).

The antitumor efficacy study showed that the ultrasound exposure over the right tumor enhanced growth inhibition. As tumors were grown on both flanks but only the right tumor

Downloaded from jpet.aspetjournals.org at ASPET Journals on April 10, 2024

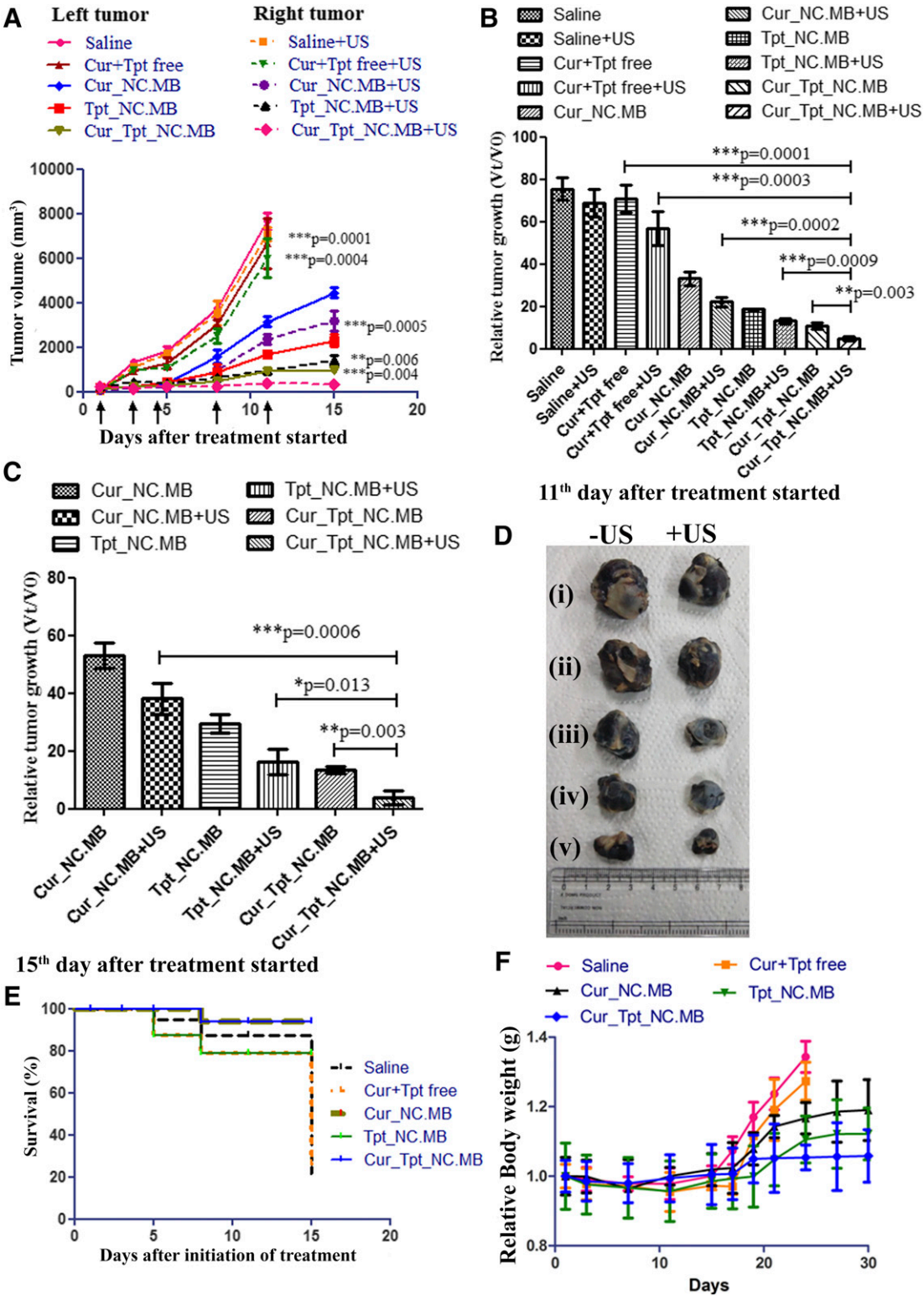

Fig. 12. (A) Regression of tumor volume in different groups of treatments. (B) Relative tumor growth at the end of 11th day after treatment started. (C) Relative tumor growth at the end of 15th day after treatment started. (D) Photograph showing reduction in tumor size in treatment groups: (i) saline, (ii) Cur+Tpt free, physical mixture of Cur and Tpt, (iii) Cur_NC.MB, (iv) Tpt_NC.MB, (v) Cur_Tpt_NC.MB. +US stands for the right tumor exposed to ultrasound, whereas −US stands for left tumor not exposed with ultrasound. (E) Kaplan-Meier survival analysis. (F) Change in body weight of mice during course of treatment. Results are shown as mean ± S.D. and *P* value was calculated by Student's *t* test. Cur+Tpt free, physical mixture of Cur and Tpt; US, ultrasound exposure at 50% duty cycle, 2 W/cm^2 intensity for 60 seconds.

was exposed to ultrasound, the reduction in tumor volume or relative tumor growth inhibition was higher in the right tumor. Ultrasound application would have disrupted the whole Cur_Tpt_NC.MB assembly as a result of inertial cavitation and generated secondary harmonics that would have disrupted the endothelial membrane (Fig. 13). Compromised

Downloaded from jpet.aspetjournals.org at ASPET Journals on April 10, 2024

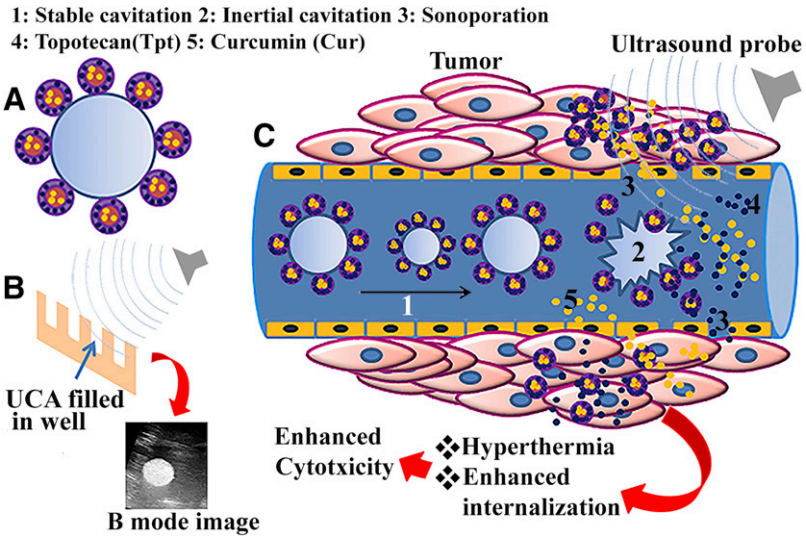

Fig. 13. (A) Nanoconjugates Cur_Tpt_NC.MB developed for ultrasound-mediated combinational therapy for cancer. (B) In presence of ultrasound these nanoconjugates undergo repetitive compression and rarefaction and generate secondary harmonics that is the basis of ultrasonographic image. (C) Owing to cumulative action of inertial cavitation and secondary harmonics, the ultrasound exposure leads to extravasation of circulating drug/drug-laden nanocarriers Cur_Tpt_NC by compromising the integrity of endothelial lining of the tumor's capillaries, which we exploited that for intratumoral delivery of anticancer drug.

endothelial lining would have created a pathway for intratumoral transport of the <200-nm-sized Cur_Tpt_NC or released Cur/Tpt (Stieger et al., 2007; Cool et al., 2013). This is explained by another result, obtained through thin-section CLSM imaging of a tumor slice, that showed the higher internalization of dye in an ultrasound-exposed tumor compared with the left flank tumor. This reveals that ultrasound pulses can permeabilize the tumor and enhance the penetration of dye. Moreover, the insonation catalyzed on-demand release and therefore facilitated both release and internalization concurrently. In addition to that, the particles internalized by the tumor in the presence of ultrasound exposure would have released the drug sustainably and induced tumor regression. Although the reduction in volume occurred significantly even in the noninsonated left tumor of the Cur_Tpt_NC.MB treatment group compared with left tumor of the group treated with a physical mixture of Cur and Tpt, this might have happened as a result of the compressible nature of nanoconjugates, which can squeeze through tumor neovasculature and enable the regression (Chandan and Banerjee, 2018). The rate of regression, however, was lower than in the right tumor. Additional factors that might play a role in reducing the tumor size include the cavitation of Cur_Tpt_NC.MB, which might release energy to break the oxygen molecule into oxide and hydroxide radicals and initiate apoptosis (Wan et al., 2016). Moreover, Tpt induces ROS generation, in turn irreversibly modifying the biomolecules, viz., protein, DNA, lipid, and carbohydrate, and leading to apoptosis (Circu and Aw, 2010). As far as change in the body weights of mice is concerned, body weight in every group decreased very minimally in the initial phase owing to injection of cells and initiation of tumor development, but later it increased gradually as the tumor rapidly grew, and that is why the increase in body weight was highest in the group treated with saline and lowest in the Cur_Tpt_NC.MB group (Chandan and Banerjee, 2018). Also, ultrasound exposure leads to localized mild hyperthermia and that would have contributed also to the reduction in tumor size by noncoagulative necrosis (Tang et al., 2015).

In conclusion, the current study demonstrates that the nanoconjugate Cur_Tpt_NC.MB has great potential as an ultrasound-triggered dual-drug delivery carrier for spatiotemporal combination therapy of cancer.

Acknowledgments

The authors acknowledge the Indian Institute of Technology Bombay (IIT Bombay) for providing access to the research facilities and are grateful to the Sophisticated Analytical Instrument facility and Industrial Research and Consultancy Centre, IIT Bombay, for providing instrumental facilities. C.P. is grateful to the Department of Biotechnology, Ministry of Science and Technology, Government of India, for junior and senior research fellowships.

Authorship Contributions

Participated in research design: Prasad, Banerjee.
Conducted experiments: Prasad.
Wrote or contributed to the writing of the manuscript: Prasad, Banerjee.

References

Bartczak D and Kanaras AG (2011) Preparation of peptide-functionalized gold nanoparticles using one pot EDC/sulfo-NHS coupling. *Langmuir* **27**:10119–10123.
Bohari SPM, Aboulkheyr H, Nur ES, Johan S, and Zianudin NF (2017) Low intensity ultrasound induced apoptosis in MCF -7 breast cancer cell lines. *Sains Malays* **46**: 575–581.
Chandan R and Banerjee R (2018) Pro-apoptotic liposomes-nanobubble conjugate synergistic with paclitaxel: a platform for ultrasound responsive image-guided drug delivery. *Sci Rep* **8**:2624.
Circu ML and Aw TY (2010) Reactive oxygen species, cellular redox systems, and apoptosis. *Free Radic Biol Med* **48**:749–762.
Cool SK, Geers B, Roels S, Stremersch S, Vanderperren K, Saunders JH, De Smedt SC, Demeester J, and Sanders NN (2013) Coupling of drug containing liposomes to microbubbles improves ultrasound triggered drug delivery in mice. *J Control Release* **172**:885–893.
Cosgrove D (2006) Ultrasound contrast agents: an overview. *Eur J Radiol* **60**: 324–330.
Dobrovolskaia MA, Aggarwal P, Hall JB, and McNeil SE (2008) Preclinical studies to understand nanoparticle interaction with the immune system and its potential effects on nanoparticle biodistribution. *Mol Pharm* **5**:487–495.
Drummond DC, Noble CO, Guo Z, Hayes ME, Connolly-Ingram C, Gabriel BS, Hann B, Liu B, Park JW, Hong K, et al. (2010) Development of a highly stable and targetable nanoliposomal formulation of topotecan. *J Control Release* **141**:13–21.
Escoffre JM, Mannaris C, Geers B, Novell A, Lentacker I, Averkiou M, and Bouakaz A (2013) Doxorubicin liposome-loaded microbubbles for contrast imaging and ultrasound-triggered drug delivery. *IEEE Trans Ultrason Ferroelectr Freq Control* **60**:78–87.
Fassberg J and Stella VJ (1992) A kinetic and mechanistic study of the hydrolysis of camptothecin and some analogues. *J Pharm Sci* **81**:676–684.
Feng Y, Tian Z, and Wan M (2010) Bioeffects of low-intensity ultrasound in vitro: apoptosis, protein profile alteration, and potential molecular mechanism. *J Ultrasound Med* **29**:963–974.
Ferrara KW (2008) Driving delivery vehicles with ultrasound. *Adv Drug Deliv Rev* **60**:1097–1102.
Geers B, Lentacker I, Sanders NN, Demeester J, Meairs S, and De Smedt SC (2011) Self-assembled liposome-loaded microbubbles: the missing link for safe and efficient ultrasound triggered drug-delivery. *J Control Release* **152**:249–256.
Gottstein C, Wu G, Wong BJ, and Zasadzinski JA (2013) Precise quantification of nanoparticle internalization. *ACS Nano* **7**:4933–4945.

Downloaded from jpet.aspetjournals.org at ASPET Journals on April 10, 2024

Jain S, Rathi VV, Jain AK, Das M, and Godugu C (2012) Folate-decorated PLGA nanoparticles as a rationally designed vehicle for the oral delivery of insulin. *Nanomedicine (Lond)* **7**:1311–1337.
Kurita T and Makino Y (2013) Novel curcumin oral delivery systems. *Anticancer Res* **33**:2807–2821.
Lentacker I, Geers B, Demeester J, De Smedt SC, and Sanders NN (2010) Design and evaluation of doxorubicin-containing microbubbles for ultrasound-triggered doxorubicin delivery: cytotoxicity and mechanisms involved. *Mol Ther* **18**:101–108.
Li Y, Wang P, Zhao P, Zhu S, Wang X, and Liu Q (2012) Apoptosis induced by sonodynamic treatment by protoporphyrin IX on MDA-MB-231 cells. *Ultrasonics* **52**:490–496.
Liu HL, Fan CH, Ting CY, and Yeh CK (2014) Combining microbubbles and ultrasound for drug delivery to brain tumors: current progress and overview. *Theranostics* **4**:432–444.
Lv Y, Hao L, Hu W, Ran Y, Bai Y, and Zhang L (2016) Novel multifunctional pH-sensitive nanoparticles loaded into microbubbles as drug delivery vehicles for enhanced tumor targeting. *Sci Rep* **6**:29321.
Morelli C, Maris P, Sisci D, Perrotta E, Brunelli E, Perrotta I, Panno ML, Tagarelli A, Versace C, Casula MF, et al. (2011) PEG-templated mesoporous silica nanoparticles exclusively target cancer cells. *Nanoscale* **3**:3198–3207.
Mosmann T (1983) Rapid colorimetric assay for cellular growth and survival: application to proliferation and cytotoxicity assays. *J Immunol Methods* **65**:55–63.
Mura S, Nicolas J, and Couvreur P (2013) Stimuli-responsive nanocarriers for drug delivery. *Nat Mater* **12**:991–1003.
Muzzarelli RAA (1998) Colorimetric determination of chitosan. *Anal Biochem* **260**: 255–257.
Ordeig O, Chin SY, Kim S, Chitnis PV, and Sia SK (2016) An implantable compound-releasing capsule triggered on demand by ultrasound. *Sci Rep* **6**:22803.
Petschauer JS, Madden AJ, Kirschbrown WP, Song G, and Zamboni WC (2015) The effects of nanoparticle drug loading on the pharmacokinetics of anticancer agents. *Nanomedicine (Lond)* **10**:447–463.
Qin S, Caskey CF, and Ferrara KW (2009) Ultrasound contrast microbubbles in imaging and therapy: physical principles and engineering. *Phys Med Biol* **54**:R27–R57.
Rao W, Zhang W, Poventud-Fuentes I, Wang Y, Lei Y, Agarwal P, Weekes B, Li C, Lu X, Yu J, et al. (2014) Thermally responsive nanoparticle-encapsulated curcumin and its combination with mild hyperthermia for enhanced cancer cell destruction. *Acta Biomater* **10**:831–842.
Sirsi SR and Borden MA (2012) Advances in ultrasound mediated gene therapy using microbubble contrast agents. *Theranostics* **2**:1208–1222.
Stewart JCM (1980) Colorimetric determination of phospholipids with ammonium ferrothiocyanate. *Anal Biochem* **104**:10–14.
Stieger SM, Caskey CF, Adamson RH, Qin S, Curry FR, Wisner ER, and Ferrara KW (2007) Enhancement of vascular permeability with low-frequency contrast-enhanced ultrasound in the chorioallantoic membrane model. *Radiology* **243**:112–121.
Tang J, Guha C, and Tomé WA (2015) Biological effects induced by non-thermal ultrasound and implications for cancer therapy: a review of the current literature. *Technol Cancer Res Treat* **14**:221–235.
Tiwari SK, Agarwal S, Seth B, Yadav A, Nair S, Bhatnagar P, Karmakar M, Kumari M, Chauhan LK, Patel DK, et al. (2014) Curcumin-loaded nanoparticles potently induce adult neurogenesis and reverse cognitive deficits in Alzheimer's disease model via canonical Wnt/β-catenin pathway. *ACS Nano* **8**:76–103.
Vareed SK, Kakarala M, Ruffin MT, Crowell JA, Normolle DP, Djuric Z, and Brenner DE (2008) Pharmacokinetics of curcumin conjugate metabolites in healthy human subjects. *Cancer Epidemiol Biomarkers Prev* **17**:1411–1417.
Wan GY, Liu Y, Chen BW, Liu YY, Wang YS, and Zhang N (2016) Recent advances of sonodynamic therapy in cancer treatment. *Cancer Biol Med* **13**:325–338.
Wang X, Gao Y, Wang W, Qin A, Sun JZ, and Tang BZ (2016) Different amine-functionalized poly (diphenylsubstituted acetylenes) from the same precursor. *Polym Chem* **7**:5312–5321.
Xing Z, Ke H, Wang J, Zhao B, Yue X, Dai Z, and Liu J (2010) Novel ultrasound contrast agent based on microbubbles generated from surfactant mixtures of Span 60 and polyoxyethylene 40 stearate. *Acta Biomater* **6**:3542–3549.
Zhou Y, Yang K, Cui J, Ye JY, and Deng CX (2012) Controlled permeation of cell membrane by single bubble acoustic cavitation. *J Control Release* **157**:103–111.
Zhu X, Guo J, He C, Geng H, Yu G, Li J, Zheng H, Ji X, and Yan F (2016) Ultrasound triggered image-guided drug delivery to inhibit vascular reconstruction via paclitaxel-loaded microbubbles. *Sci Rep* **6**:21683.

Address correspondence to: Dr. Rinti Banerjee, Department of Biosciences and Bioengineering, Indian Institute of Technology, Bombay, Mumbai, India. E-mail: rinti@iitb.ac.in

Downloaded from jpet.aspetjournals.org at ASPET Journals on April 10, 2024

SUPPLEMENTAL DATA

Ultrasound Triggered Spatiotemporal Delivery of Topotecan and Curcumin as Combination Therapy for Cancer

Chandrashekhar Prasad[1] and Rinti Banerjee [1,*]

[1]Department of Biosciences and Bioengineering, Indian Institute of Technology, Bombay, Mumbai, India

[*]Corresponding author: Department of Biosciences and Bioengineering, Indian Institute of Technology, Bombay, Mumbai, India. Email ID: rinti@iitb.ac.in, Phone Number: +9122 2576 7868

Journal of pharmacology and experimental therapeutics

Supplemental Figures

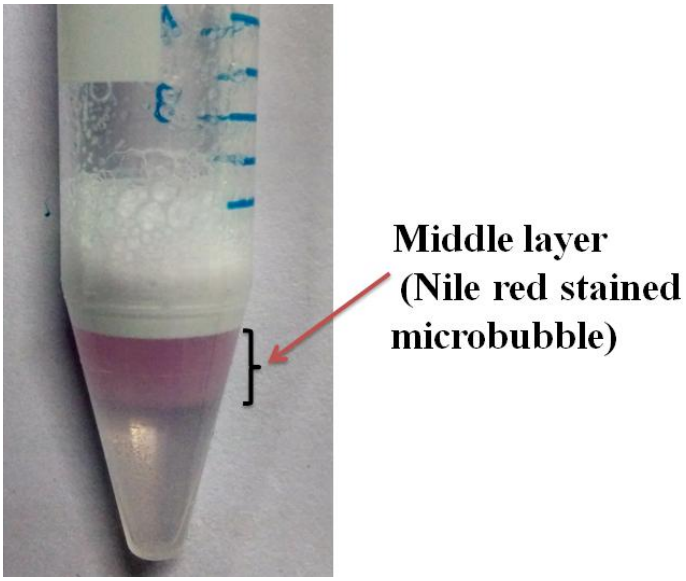

Figure S.1 Three layers separation of MB suspension. Middle layer of suspension shows nile red stained MB (MB-ND).

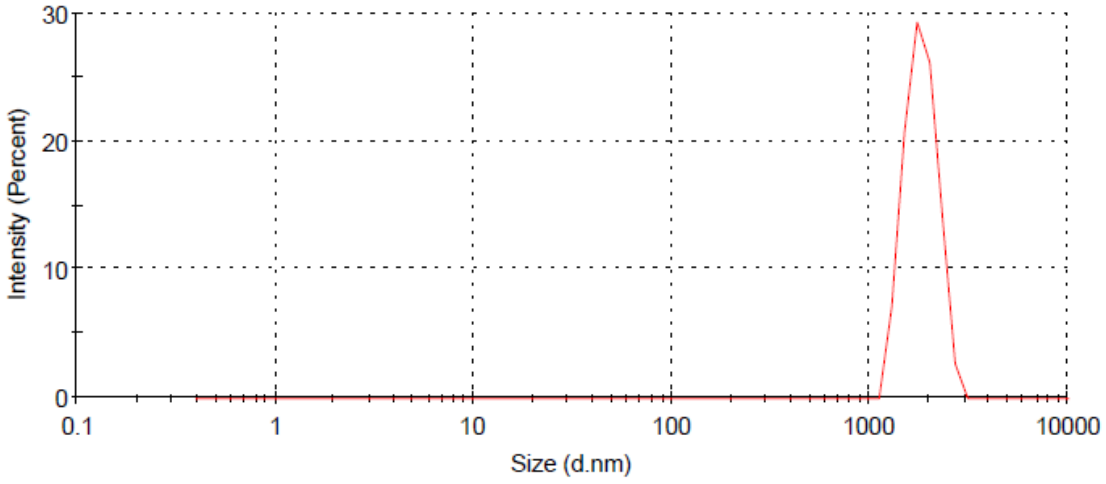

Figure S.2. Hydrodynamic diameter range of Cur_Tpt_NC.MB.

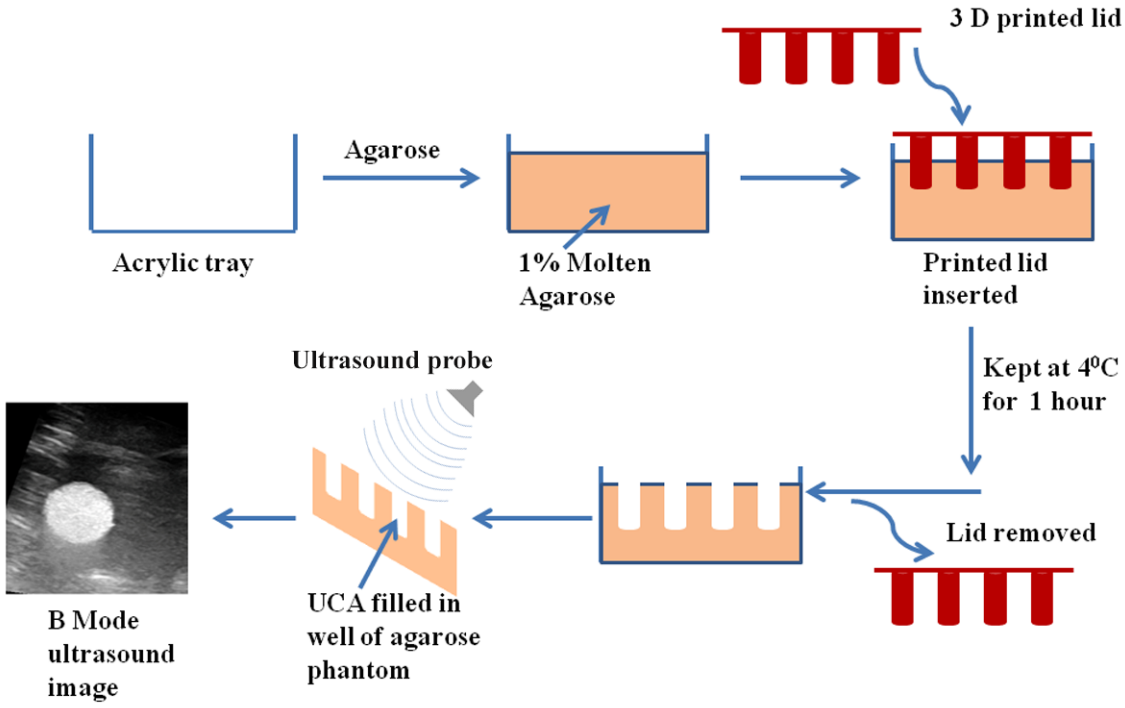

Figure S.3 Schematic presentation of preparation of agarose phantom.

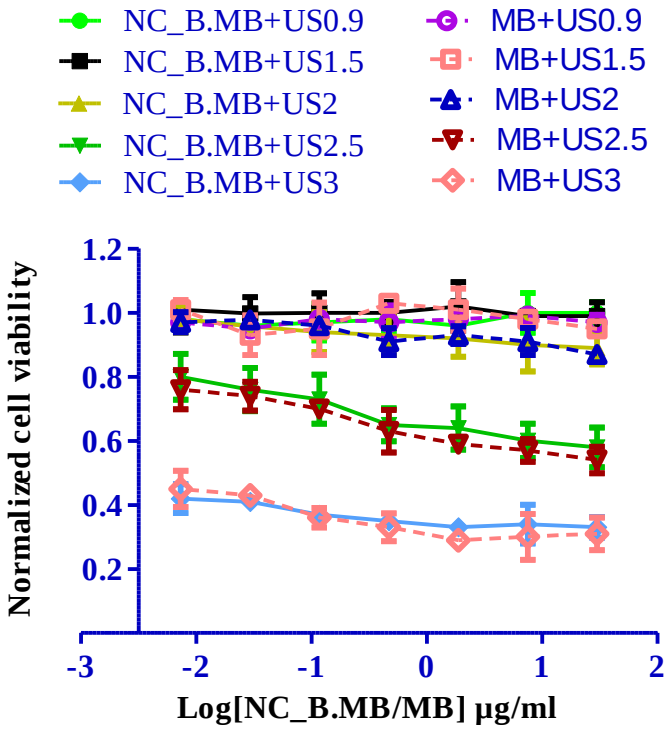

Figure S.4 Decrease in cell viability of MDA MB 231 cells in presence of NC_B.MB and MB (at concentration 0.007-30 µg/ml, with respect to MB) with ultrasound exposure at fixed duty cycle 50% for fixed time 15 sec with increasing intensity 0.9, 1.5, 2, 2.5 and 3 W/cm^2.

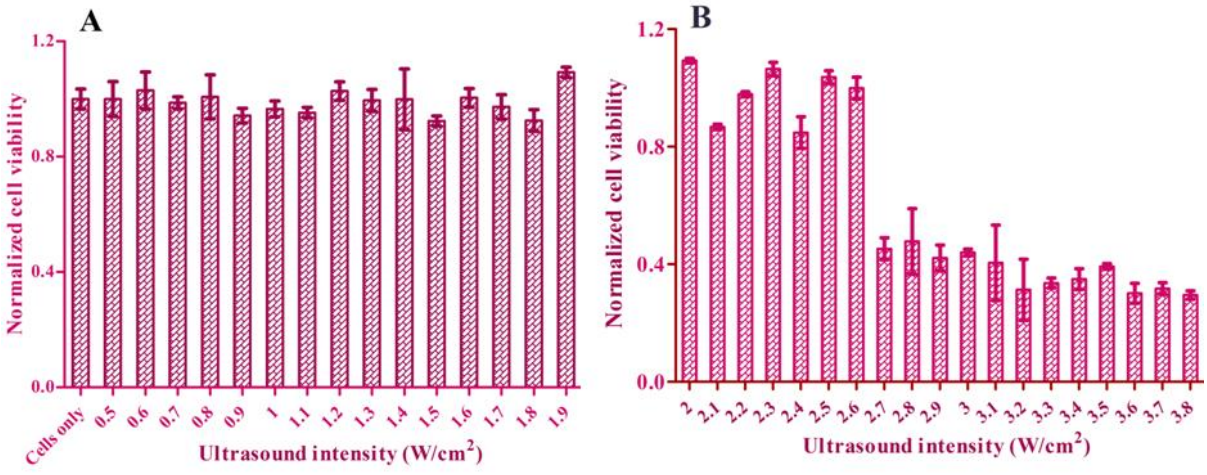

Figure S.5 Ultrasound intensity and its effect on cell viability in absence of MB and nanoconjugates Cur_Tpt_NC.MB at fixed duty cycle 50% and time period 15 sec, (A) intensity varying from 0.5 - 1.9 W/cm^2, (B) intensity varying from 2-3.8 W/cm^2.

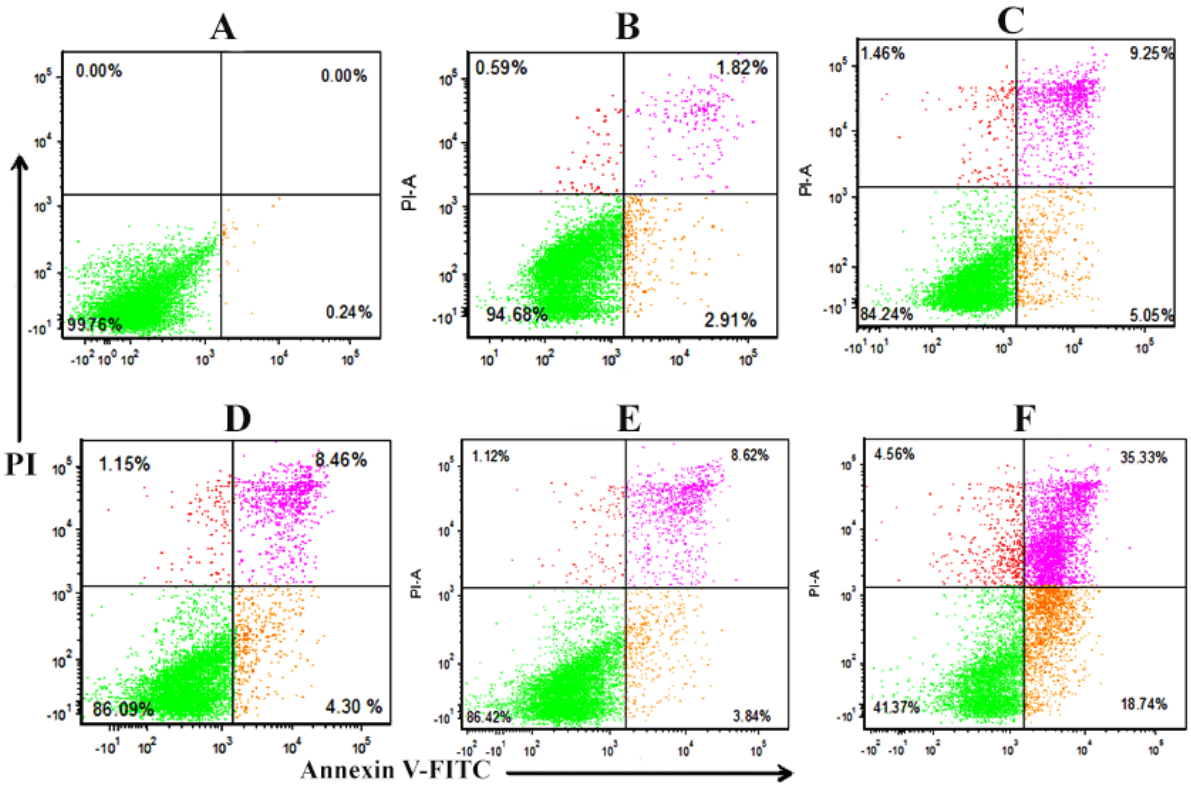

Figure S.6 Treatment with ultrasound in presence of Tpt_NC.MB increased the percentage of both early and late apoptotic cells. (A) Only cells without staining with PI and annexin V-FITC. (B) Cells were not treated but stained with PI and annexin V-FITC. (C) Treated with Tpt. (D) Treated with Tpt_NC. (E) Treated with Tpt_NC.MB. (F) Treated with Tpt_NC.MB+US2 (ultrasound exposure at 2 W/cm^2 intensity, 50% duty cycle, 15 sec time period).

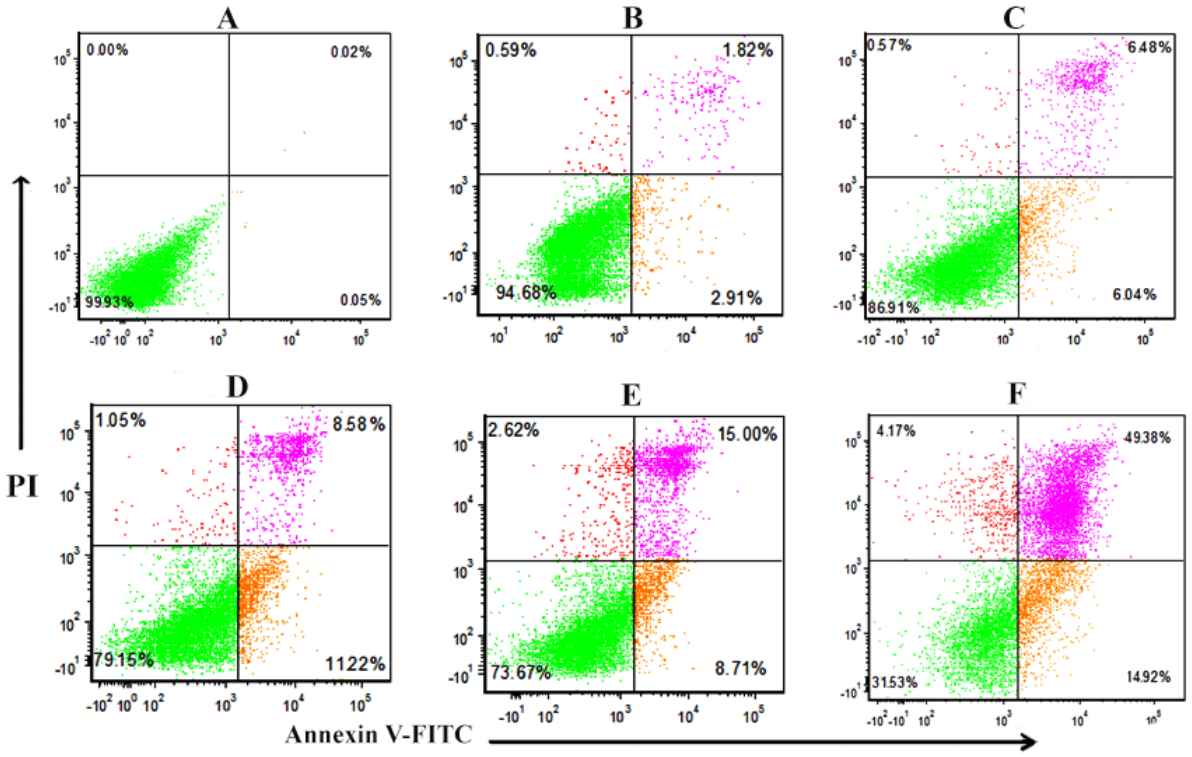

Figure S.7 Treatment with ultrasound in presence of Cur_NC.MB increased the percentage of both early and late apoptotic cells. (A) Only cells without staining with PI and annexin V-FITC. (B) Cells were not treated but stained with PI and annexin V-FITC. (C) Treated with Cur. (D) Treated with Cur_NC. (E) Treated with Cur_NC.MB. (F) Treated with Cur_NC.MB+US2 (ultrasound exposure at 2 W/cm^2 intensity, 50% duty cycle, 15 sec time period).

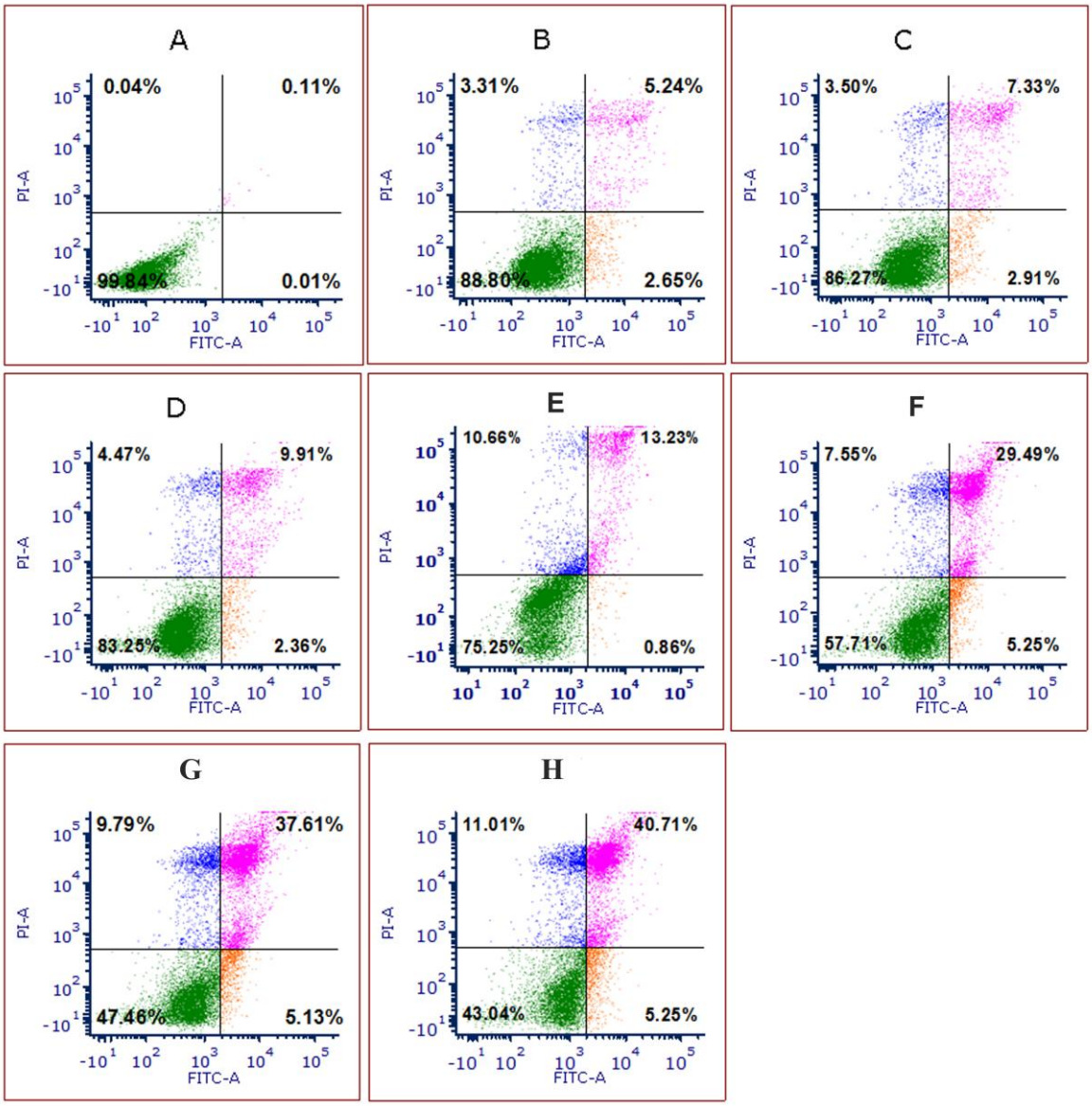

Figure S.8 Treatment with ultrasound and additive effect between Tpt (50 nM) and Cur (100 nM) enhanced the total sum of apoptotic and necrotic cells as compared to individual free drug and their physical mixture. (A) Only cells (B) Cur free (C) Tpt free (D) Cur+Tpt free mixture (E) Cur_Tpt_NC (F) Cur_NC.MB+US2 (G) Tpt_NC.MB+US2 (H) Cur_Tpt_NC.MB+US2. In data acquisition, PI-A channel was used for propidium iodide and FITC-A for annexin V-FITC.

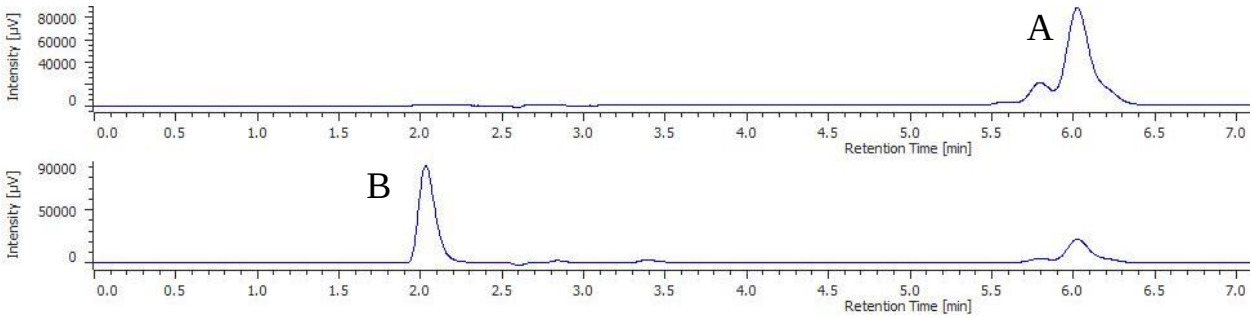

Figure S.9 HPLC chromatogram of 1 µg/ml drug shows intensity (µV) vs. retention time (min), (A) Cur, (B) Tpt.

Table S.1 DLS, Zeta potential and encapsulation efficiency of nanoparticle.

Nanoparticles	**Lecithin: Cur (wt:wt)**	**Chitosan: Tpt (wt:wt)**	**Encapsulation efficiency (%) Tpt/Cur**	**Size (nm)**	**Zeta potential (mV)**
Cur_NE	13:1			60.5±8.3	-39.3±6.8
Cur_NE	8:1			55.5±7.2	-35.6±9.5
Cur_Tpt_NC	13:1	2:1	27.5±2.7/44.5±2.9	163.7±5.1	+27.6±3.8
Cur_Tpt_NC	8:1	1:1	35±4.4/60.6±4.3	170.9±20.3	+23.3±5.7
MB	-	-	-	1200.6±201.8	-15.9±4.8
Cur_Tpt_NC.MB			33.1±2.3/58.32±2.9	1760.4± 350.3	-12.7±2.3

Table S.2 Amount of Tpt and Cur in different vital organs (in ng/g of tissue).

Organs	**Cur_Tpt_NC.MB (Tpt)**	**Cur_Tpt_NC.MB (Cur)**	**Cur**	**Tpt**
Liver	2801.2±362.3	2517.4±330.6	521.3±12.4	1081.1±234.5
Kidney	1289.3±282.7	1454.9±376.2	123.2±21.6	451.6±127.3
Spleen	1541.6±341.9	1265.6±298.7	451.4±33.9	694.2±234.1
Brain	432.1±103.5	451.5±119.2	103.7±55.2	45.9±12.7
Lung	781.7±329.4	762.4±234.1	172.5±67.1	243.4±16.4
Heart	2123.5±333.8	1576.5±451.7	251.6±23.7	842.7±123.1
Peyer's patch	1002.4±129.1	1308.3±121.7	136.7±21.8	456.2±98.5

Table S.3 MTD of the free drug and nanoconjugates Cur_Tpt_NC.MB in C57BL/6 mice.

Cur/Tpt dose (mg)/kg body weight	**Cur+Tpt free**	**Cur_Tpt_NC.MB**
20/10	Alive	Died just after injection
10/5	Alive	Alive but became dormant for some time
5/2.5	Alive	Alive and active